Measurement of the visual perceptibility of sink marks in injection molded parts

Master's Thesis by

DIETMAR HABA

Polymer Competence Center Leoben GmbH
and
Chair of Polymer Processing, Montanuniversitaet Leoben

Leoben, May 2011

Dietmar Haba: *Measurement of the visual perceptibility of sink marks in injection molded parts,* Master's Thesis, © May 2011

SUPERVISOR:
Dipl.-Ing. Dr.techn. Dieter P. Gruber

ASSESSOR:
Univ.Prof. Dipl.-Ing. Dr.mont. Clemens Holzer

LOCATION:
Leoben

TIME FRAME:
May 2011

Essentially, all models are wrong, but some are useful.

— George E. P. Box

ACKNOWLEDGMENTS

The research work of this Master's Thesis was performed at the Polymer Competence Center Leoben GmbH (PCCL, Austria) within the framework of the K_{plus}-program of the Austrian Ministry of Traffic, Innovation and Technology with contributions by the University of Leoben (*Institute for Plastics Processing*). The PCCL is funded by the Austrian Government and the State Governments of Styria and Upper Austria.

SPECIAL THANKS GO TO:
Dipl.-Ing. Dr.techn. Dieter P. Gruber
for guidance, advice during work and supervision of the master's thesis.

Univ.Prof. Dipl.-Ing. Dr.mont. Clemens Holzer
for assessing the thesis.

Special thanks go to Dipl.-Ing. Johannes Macher for his continuous backup during execution and reporting as well as for his valuable advices.
Similarly, much thanks to Dipl.-Ing. Gernot Pacher, who did great preliminary work and assisted with making this thesis.

ABSTRACT

The aim of this work was to contribute to the improvement of a methodology for the evaluation of the visual perceptibility of sink marks on surfaces of injection molded parts by machine vision. Based on previous research work on the detection of surface defects a new methodology for the evaluation of the visibility of sink marks using digital images was developed. The methodology uses a surface model to approximate the intensity matrix of captured images. Calculated surface fit functions were used to determine the amplitudes of the second derivatives (ASD) for quantifying the perceptibility of the sink marks. Injection molding parts produced by using different predefined processing parameters were inspected and the influence of given parameters on the visual perceptibility of the sink marks was evaluated. ASD emerged to be an appropriate parameter for the application in a machine vision system. The results partly contradict findings of other authors.

KURZFASSUNG

Das Ziel dieser Arbeit war es, beizutragen zur Verbesserung einer Methodik zur Evaluierung der visuellen Wirksamkeit von Einfallstellen auf Oberflächen von Spritzgussteilen durch maschinelles Sehen. Basierend auf vorhergehender Forschungsarbeit zur Erkennung von Oberflächenfehlern wurde eine neue Methodik zur Evaluierung der Sichtbarkeit von Einfallstellen mittels digitaler Bilder entwickelt. Die Methodik verwendet ein Flächenmodell um die Amplituden der zweiten Ableitungen (ASD) zur Messung der Wahrnehmbarkeit von Einfallstellen zu bestimmen. Spritzgussteile, die mit verschiedenen, vorgegebenen Prozessparametern produziert worden waren, wurden inspiziert und der Einfluss gegebener Parameter auf die visuelle Wirksamkeit von Einfallstellen wurde evaluiert. Der ASD entpuppte sich als adäquater Parameter zur Anwendung in einem System zum maschinellen Sehen. Die Ergebnisse widersprechen zum Teil den Erkenntnissen anderer Autoren.

CONTENTS

1 INTRODUCTION AND MOTIVATION

Injection molding has become an important process in high-quality industries. As a lot of injection molded products are visible front parts, injection molding has to deal with surface quality assurance. Especially if parts are to be processed further it is highly necessary to eliminate bad parts as soon as possible. Thereby, further processing costs can be reduced considerably. As long as defects are not critical, a grading of commodities can be useful.
There are a lot of factors that influence a part's visual appearance. Besides the material and the tool properties, injection parameters have huge influence on the visibility of surface defects. Due to given design limits, consequences on surface quality are ignored during design stages in many cases and it is demanded only from the producer to avoid them. Description of the injection molding process is given in Section 3.1.1 in this work.

This work is aimed on the quantitative characterization of the *visibility of sink marks*. Sink marks are a common surface defect in injection molding parts. Indeed, sink marks do not affect a part's mechanical properties, but they make parts look of lower quality. As high-quality industry tries to avoid sink marks they have become an indicator for a non-valuable production – all the more it is necessary to avoid them. When prevention of sink marks is not possible, it is necessary to evaluate their perceptibility to minimize their visibility.
Sink mark formation is conditioned by machine settings that influence shrinking, as holding pressure, injection fill rate or temperatures. Description of sink marks and their prevention is given in Section 3.2.
Modern software makes it easy to precalculate possible appearance of sink marks, whereby potential sink mark locations can be predicted. Both occurrence and severity can be predicted [1–7]. But even by thorough tooling sink marks are not completely avoidable in many cases. It is important to be aware of their strength of perceptibility.

It was the objective of this work to contribute to the development of a methodology for quantifying the visual perceptibility of sink marks based on machine vision and image processing, where the measurements are demanded to correlate with human perception. Furthermore, results must be precise, non-ambiguous and reproducible.
It is assumed that an efficient methodology to evaluate sink mark visibility would appeal to high-quality industry and would be applied in a series of applications.

The following substantial work was published in the area of inspection of plastics surfaces and prediction of sink marks, respectively:

Flow simulation in combination with finite element analysis were used by Shi and Gupta to predict location and depth of sink marks published in several papers. They included temperatures and cavity pressures in their work. Experiments show the trends predicted by the simulation model. [2–7]

Neural networks were used by various authors to model injection molding defects. It was found that they can be used instead of traditional computational flow analysis. Applying the neural networks reduced the amount of computational time and the pre- and post-processing time as compared to simulation methods. [8, 9]

Ni used CAE injection molding simulation programs to describe the dominant factors causing sink marks and compared his findings with measurements of an actual injection molded part. The predictions were in good agreement with experiments and pointed out that the higher thermal mass and the effective packing time near a rib base are determining parameters for the depth of a sink mark. Also, he found influences of the used material, the part's geometry, the cooling channel layout and the molding process windows. [10]

Mérillou et al. engaged in measurement of surface scratches in different materials. They combined the bidirectional reflectance distribution function (BRDF) with usual texture mapping, whereby they drew the bow from geometrical measuring of a surface and its visual perceptibility. [11]

Automatic visual inspection of surface defects is not only used in polymer engineering. Pernkopf and O'Leary experimented with surface reflectance of metallic surfaces to maximize the contrast between errors and intact surface. They presented a prototype of an automatic system for surface inspection. [12]

Silvennoinen et al. published several works about measurement of gloss differences on injection molded parts and other surfaces. They presented a method to measure gloss on convex or concave surfaces. [13]

Proceedings in measurement of visual appearance of sink marks were made by Hayden and Engelmann. They investigated visibility of sink marks statistically in the course of a field study and developed new guidelines for determining a texture depth to hide sink marks. [14, 15]

Li et al. measured visual appearance of weld lines in injection molded parts. The visual appearance was evaluated by analyzing differences in the hue values of digital images of the defects. [16]

In 2008, Xie gave a detailed review about advances in surface defect detection in the previous years. [17]

Mathivanan and Parthasarathy simulated injection molding processes and calculated resulting depth of the sink marks. *Based on fractional factorial design (FFD)*, most influential injection molding variables were selected. Afterwards, *central composite design (CCD) of experiments* was used to formulate a predictive nonlinear model. [18]

There are numerous publications about visual inspection of surfaces, but the direct measurement of visibility of sink marks on injection molded parts has not yet been explored well.

This work is based on the work of Gruber who developed a methodology to calculate quantitative values for the perceptibility of surface defects. In a preliminary thesis Pacher was using the *amplitude of the second derivative (ASD)* of an intensity profile perpendicular to the sink mark to derive a parameter for sink mark detection and compared measurement results with topographical measurements. Gruber and Pacher found ASD to be a model parameter that fits visual perception very well. [19–22]

The course of the given work included the injection molding of test specimens under varying processing conditions, leading to parts with differently obvious local sink marks at the opposite site of a pin on the test part. Thereby, CCD-images were acquired of the sink marks in a way that ensures maximum defect contrast. Images were pre-processed to improve their processibility. Subsequently, a model was derived in order to get a mathematical representation from sink marks out of the acquired images. Using this model, a quantitative value for the perceptibility of the sink marks was derived that can be used to measure the visual perceptibility of the sink marks. The methodology was tested by given specimens.

2

BASICS OF IMAGE PROCESSING

This section is to show the fundamentals of image processing used in this work. A short overview is given below:

In Section 2.1 the most important principles of digital image representation are described. Section 2.1.1 includes the principles of image acquisition by digital cameras. Section 2.1.2 illustrates the principles, how a digital image is represented.

In Section 2.2 important image processing methods are described. This section covers filtering of digital images (Section 2.2.1) and surface fitting (Section 2.2.2).

2.1 DIGITAL IMAGE REPRESENTATION

2.1.1 *Image acquisition using digital cameras*

Digital cameras applied in this work are equipped with charge-coupled device (CCD)-photosensors, which are arrays of little devices that are photosensitive and able to transform the incident light into electric charge. When illuminated for a certain period of time each device receives an amount of charge proportional to the integral of the light energy projected onto its surface. For readout, the charge of each little device is passed to its neighbor in one direction. At one certain device, the charge is picked off and converted into digital information. Modern CCD-cameras use sensors with 4000 × 4000 CCD-elements and more. For further information about CCD-sensors, Gonzales and Woods give a good introduction. [23]

The first function of a digital camera is to collect the incident light and direct it in a focused form onto the image plane (sensor). This is done by the lens of the camera. The sensor array is positioned to receive the light, convert it into an electrical signal and to pass this through for conversion to a digital image. [23]

Figure 1 illustrates how the number of CCDs in the sensor influences the quality of the image. Although the figure is darker in its outer edges, it seems to become brighter there in the digital image. This is due to the white background of the object and the anti-aliasing at the edge of the object.

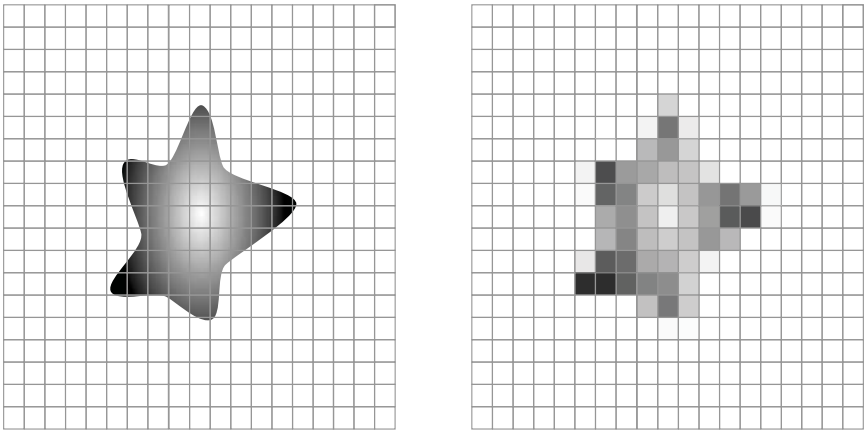

(a) illuminated sensor (b) resulting image

Figure 1: An illuminated CCD-sensor and the resulting image. The number of pixels is too low to achieve acceptable resolution.

2.1.2 *Spatial representation of digital images*

To process images it is necessary to find a representation that a computer can deal with. Image information needs to be converted to two-dimensional, discrete arrays of points. One point is called *pixel* (which is the abbreviation of *picture element*). A pixel represents the mean irradiation of a certain square area of the image. Normally, pixels are distributed on a rectangular grid. Their position among this grid is given by indices. The first index, m, denotes the pixels' row position, the second one, n, denotes their column position. In accordance with its matrix notation, the vertical axis of a digital image runs from top to bottom. The horizontal axis runs from left to right. In Figure 2 an image array and the definition of a certain pixel are illustrated. The more pixels an image is composed of, the higher its resolution and the required memory is. [24]

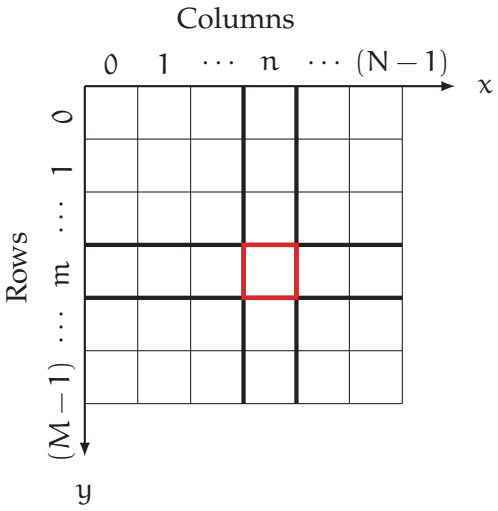

Figure 2: Representation of an image by an rectangular array of pixels with M rows and N columns.

For computer processing the measured irradiance at a certain point must be mapped onto a limited number Q of brightness levels. This process is called *quantization*. Q is calculated from the *bit depth* k, the number of bits per pixel. As computers work binary, thus in powers of 2, Q will also be a power of 2. An 8-bit picture's pixels has $Q = 2^8 = 256$ possible gray levels, a 12-bit picture's pixels has $Q = 2^{12} = 4\,096$ ones, whereas they use 1.5 times the memory. Consequently, digital images are represented by matrices of numbers from 0 to 255 in 8-bit-images, by matrices of numbers from 0 to 4 095 in 12-bit-images and by matrices of numbers from 0 to 65 535 in 16-bit images respectively. Since the *relative intensity resolution* of our visual system is not better than about 2 %[1], an 8-bit image has a resolution good enough to give the illusion of a continuous change in gray values. However, to do calculations , it will be better to use higher number of gray levels. [24]

1 That is to say, there are about 50 different gray levels a human eye can discern. [24]

To calculate digital images, it is useful to convert them to a rational number in floating point format in the interval $[0, 1]$, where 0 denotes black and 1 denotes white. Thereby, the results are independent on the number of gray levels which the original image is resolved with. Rounding errors during processing do not affect the result much since they cause deviations of only ± 1 grayscale value.
Calculation of a floating point format image out of its quantization Q and out of its bit depth k is given by:

$$g(x, y) = \frac{f(x, y)}{Q} = \frac{f(x, y)}{2^k} \tag{2.1}$$

In a color picture, each pixel consists of three colors red, green and blue (in the RGB space), which are combined by additive mixture. The proportions of those three colors are called the *tristimulus values* and are denoted R, G and B, respectively. A specific color is specified by its *trichromatic coefficients* r, g and b that are defined as follows [23]:

$$r = \frac{R}{R + G + B} \tag{2.2}$$

$$g = \frac{G}{R + G + B} \tag{2.3}$$

$$b = \frac{B}{R + G + B} \tag{2.4}$$

Images represented in the RGB color model consist of three component images, one for each primary channel (cf. Figure 3). The number of bits used to represent each pixel in RGB space is called the *pixel depth*. The pixel depth of a full-color image is three times deeper than that one of a grayscale image. It needs three times the memory space of a gray level pixel with the same quantization, whereas the number of different colors that can be shown is cubed. [23]

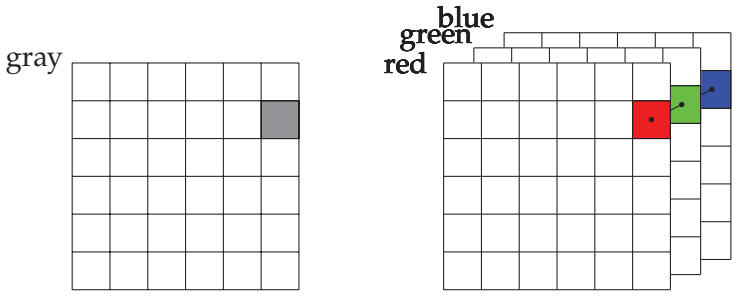

(a) grayscale image (b) RGB-image

Figure 3: A gray-scale image (a) and an RGB-image (b) in matrix forms. RGB images are three times the size of grayscale ones.

A single pixel's memory space is given by the picture's quantization and its number of channels (R, G and B) (Table 1). [24]

Table 1: Number of possible colors in dependence on the number of gray levels

Bit depth	Grayscale image		Full-color image	
	Memory	Colors	Memory	Colors
Binary	1 bit	2	3 bits	8
2 bit	2 bits	4	6 bits	64
4 bit	4 bits	16	12 bits	4 096
8 bit	8 bits	256	24 bits	$1.68 \cdot 10^7$
12 bit	12 bits	4 096	36 bits	$6.9 \cdot 10^{10}$
16 bit	16 bits	65 536	48 bits	$2.8 \cdot 10^{14}$

Converting a color image to a grayscale one can work in different manners, delivering different results, depending on which kind of value for the brightness is intended. For example, *illuminance* I of an RGB-color image is calculated simply by $I = \frac{R+G+B}{3}$ [23]. Thus, the illuminance of each pixel becomes the mean of the illuminance of this pixel's three colors.
In contrast, *luminance* or *luma* is defined as $Y = 0.3R + 0.59G + 0.11B$. This is because the human eye is most sensitive to green, then red, and least blue. This means that for equal amounts of green and blue in an image the green light will seem to be much brighter. So, the mentioned formula gives a grayscale image that appears to be altered less than one produced simply by the mean of red, green and blue.
Other possibilities to calculate a grayscale image are the *desaturation* of the image or the *decomposing* [25].

2.2 METHODS IN IMAGE PROCESSING

2.2.1 *Spatial filtering*

In order to perform surface characterization based on digital images it is necessary to do some preprocessing to reduce errors. Errors in images can be under- or overexposure, blur, poor contrast, signal noise, and others. Most of the occurring errors must be avoided by correct instrumental setup and image acquisition to guarantee good image quality.
The aim of image processing is to calculate an image matrix from raw data that allows further analysis.

During spatial filtering each pixel in an image matrix is modified in dependence on a filter mask. By using the example of a neighborhood filtering this process can be denoted by the following expression, where $f(x,y)$ denotes a given image, $g(x,y)$ denotes the processed image and T denotes an operator on f, defined over the neighborhood of (x,y).

$$g(x,y) = T[(f(x,y)] \tag{2.5}$$

In other words, for each point (x,y), the response of the chosen filter at that point is calculated using a defined relationship. For linear spatial filtering, which this work focuses on, the response is given by the sum of products of filter coefficients and the corresponding image pixels in the area spanned by the filter mask. The sum of the filter coefficients has to be kept 1 if the overall brightness of the image should not be altered.
For a 3×3-filter mask w used on a pixel neighborhood of $f(x,y)$ the calculation of $g(x,y)$ is

$$\begin{aligned} g(x,y) = {} & w(-1,-1)\cdot f(x-1,y-1) + w(-1,0)\cdot f(x-1,y) + \ \ldots \\ & \ldots + \cdots + x(0,0)\cdot f(x,y) + \cdots + w(1,0)\cdot f(x+1,y) + \ \ldots \\ & \ldots + w(1,1)\cdot f(x+1,y+1) \end{aligned} \tag{2.6}$$

which is the sum of products of the mask coefficients with the corresponding pixels of the image matrix [23]. In Figure 4, filtering of an image with a given filter mask is illustrated.

For a general mask, the resulting image is given by

$$g(x,y) = \sum_{i=-a}^{a} \sum_{j=-b}^{b} w(s,t)\cdot f(x+s,y+t) \tag{2.7}$$

for $x = 0...(M-1)$ and $y = 0...(N-1)$, where $a = \frac{m-1}{2}$ and $b = \frac{n-1}{2}$ [23].

There are several common masks in linear spatial filtering that can blur images, sharpen them or detect or accent edges or points in an image. The

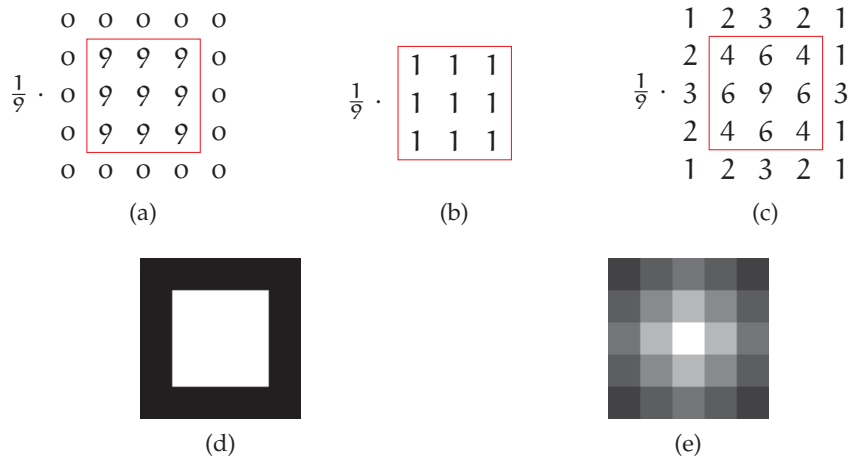

Figure 4: Spatial filtering by a 3×3-average filter. The original image matrix is shown in (a). It is filtered by an average filter in (b). The result of the filtering can be seen in (c). To depict clearly, the factor $\frac{1}{9}$ is prescinded. In (d) and (e), the image matrices (a) and (c) are shown as images. Mind that the pixel value sums of (a) and (c) are equal.

most frequently used mask works as an *average* filter. An average filter simply calculates the mean of the neighborhood of each pixel. Thereby, one has to take care to reduce noise while avoid to blur the image matrix too strongly. In this work, this filter mask is used to reduce noise as well as irrelevant detail in the image if only the major structure is of interest. The disadvantage of average filters is that they can produce false edges near strong peaks. This effect is the smaller the larger the filter mask is.

2.2.2 *Surface fitting*

Surface fitting is used in this work for the approximation of the intensity matrix of the sink mark images in the form of a function. Fitting is a mathematical optimization method to approximate the unknown parameters of a model using a list of measurement values. It is based on the idea that the principal course of the luminance values in the images is known and a surface function can be defined that describes this course well. This can be the fact if the expected images all look similar. Then the luminances of an image's pixels can be approximated through a *regression surface function*. In this work, series of images under completely equal conditions were acquired whereby all the images looked similar.
Regression is a technique for modeling several variables in order to describe given points. In a nutshell: It is possible to estimate how a value is dependent on several input variables. In contrast to regression fitting is a function approximation where measurement errors are considered. Hence, the resulting fitting parameters are also always defective. Good overview about basics of fitting using MATLAB® is given by Kiusalaas and Adam [26, 27].

In the given work, the MATLAB® function `fit` was used to approximate the given values by a function $f(x, y)$. Since MATLAB® version 2009b fitting of surfaces is also possible. The general tendency of the input data to describe a given curve can now be expressed by a continuous model function. Therefore, the input data does not necessarily need to describe the given curve. It suffices that there exists a strong tendency to describe it.

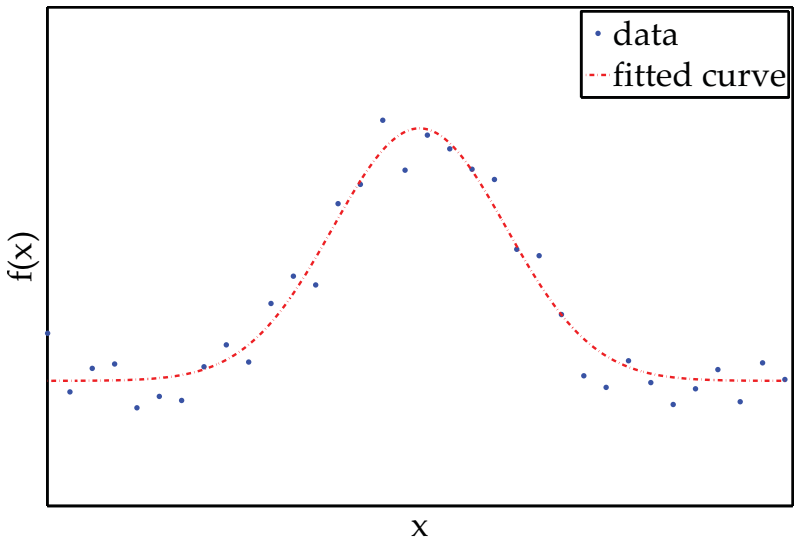

Figure 5: Example of a curve fit. The dots denote the input data, the curve denotes the Gaussian-fitted fit function.

3

EXPERIMENTAL SETUP & MEASUREMENT METHODOLOGY

In this section, the injection molding of test specimens, the formation of sink marks, the acquisition of images and the methodology of getting a quantitative value for the visibility of sink marks based on image matrices are described. Here is an overview:

In Section 3.1 injection molding of the specimens and the therefore needed equipment are presented in general. Section 3.1.1 briefly depicts the injection molding process. In Section 3.1.2 the used injection molding machine and the injection molding tool are presented. Afterwards, the used material is described in Section 3.1.3. Finally, the process latitude is introduced in Section 3.1.4.

In Section 3.2 the formation of sink marks as a surface defect with special industrial interest and its influencing parameters as well as findings of different authors are presented.

The process of image acquisition, including the photographic equipment and setup, is presented in Section 3.3.

Section 3.4 illustrates the conducted image preprocessing, namely converting images to grayscale matrices (Section 3.4.1) and reducing them to the region of interest (Section 3.4.2) as well as filtering and compressing (both in Section 3.4.3).

In Section 3.5 the fitting process is described. In Section 3.5.1 the surface fit function is derived. The chosen fit parameters are given in Section 3.5.2. In Section 3.5.3 the results of the surface fit are presented. As the fitting process takes time, depending on the used computer and the size of the image, Section 3.5.4 deals with this problem and how processing time can be limited.

In Section 3.6 it is explained, how a value for the visual perceptibility is calculated out of the fit parameters. In Section 3.6.1 it is described, how to exclude images, where no sink mark is detected. In Section 3.6.2 the calculation of the ASD out of the surface fit is illustrated.

Finally, in Section 3.7 the advantages and disadvantages of the presented methodology are discussed.

3.1 INJECTION MOLDING OF THE INVESTIGATED SPECIMENS

3.1.1 *Injection molding process*

In 2004, about 60 % of all plastics processing machines were injection molding machines [28]. According to Vines and Mukhopdhyay, injection molding consumes 32 % by weight of all plastics worldwide [29]. It has to be mentioned, that in injection molding, price per weight of material is far higher than in extrusion process. Hence, injection molding is the most important process in plastics processing in the economic sense.

Injection molding is a *net-shape* or *master forming process* that is mainly used in polymer processing of thermoplastic polymers. It enables efficient production of plastic parts in high piece numbers. In injection molding processes, hot melts of plastics are forced into cavities of the desired shapes (*molds*), where they cool down. After the product has solidified, it is demolded.

As cooling material shrinks, the final product will always be smaller than the cavity is (*shrinkage*). To decrease this effect, *holding pressure* is applied. This is the pressure that the material is compressed with after the cavity is filled, as long as the material is not yet solidified. Using too low holding pressure causes strain and high shrinkage. Too much holding pressure may cause increased internal stresses and flashes and can damage the tool. Furthermore, it is energy and therefore cost intensive.

3.1.2 *Machine & tool*

The machine used to mold the investigated specimens was an *ENGEL ES 330/80 H* with a screw diameter of 45 mm, a clamping force of 80 kN and four heating zones. [30]

The tool was for a part of the cover of a washing machine. Depending on the injection parameters, produced parts had 46 to 48 grams weight. The surface where the sink mark was expected was molded in the moving mold half.

The sink mark to analyze was a bit more than half the way the melt had to flow through inside the mold. Next to the pin that caused the sink mark there was a local diminishment of wall thickness that caused problems in image acquisition. It produced a considerable surface distortion very close to the investigated sink mark (Figure 6) due to the wall thickness diminishment on the opposite side. The formation of this surface distortion worked like the formation of a “negative sink mark” – the diminishment in wall thickness resulted in decreased shrinking compared to the rest of the part, resulting in a bulge. By diligent calibration of image acquisition and image processing it was possible to handle this problem so that the bulge did not affect the results considerably. Nevertheless, it exposed to be one of the ma-

jor problems for the surface inspection.
On the positive side the distortion caused good proof of the robustness of the methodology against unexpected surface influences. In Figure 7 the specimen with the specific region of interest is shown (cf. Section 3.4.2).

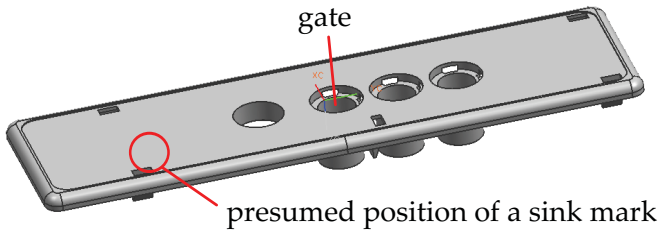

(a)

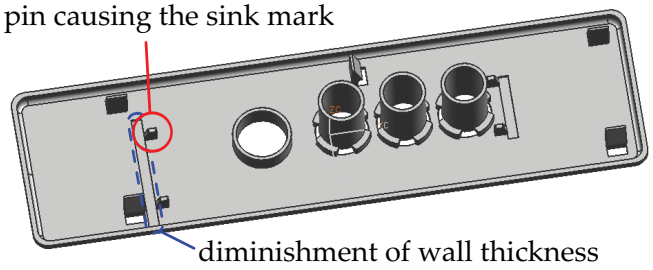

(b)

Figure 6: Drawing of the used tool, described in *Autodesk Moldflow Insight 2010*. This tool was kindly allocated by the Chair of Polymer Processing at the Montanuniversitaet Leoben (Austria).

3.1.3 *Polymer*

The chosen material was ABS *Terluran 958I*® gray, produced by BASF. Many researchers on sink marks included ABS or its alloys for their study [31]. This may be because of the prevalent use of ABS in high quality industry. The polymer properties are as mentioned in Table 2.

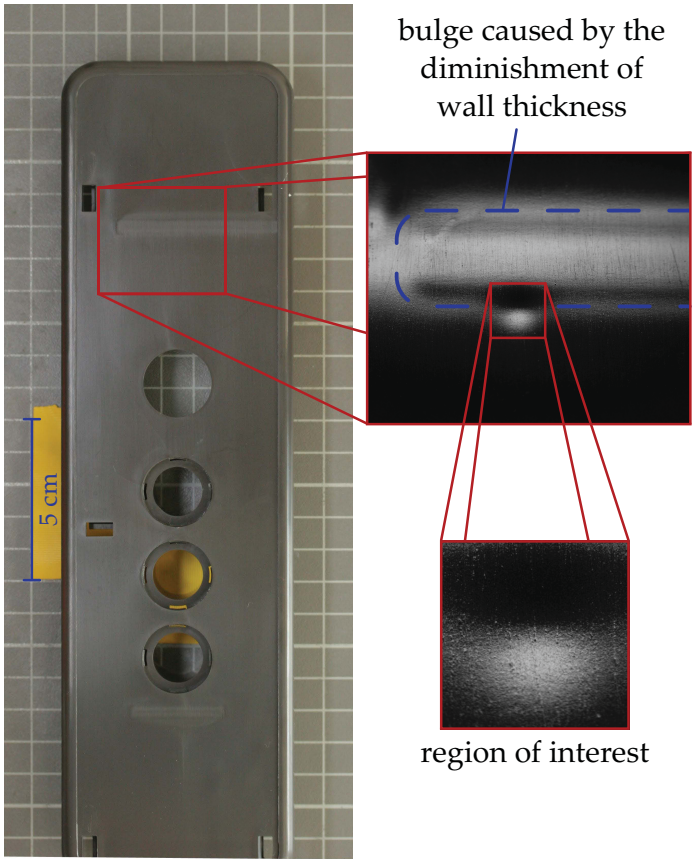

Figure 7: Image of a test part and region of interest including the investigated sink mark (cf. Section 3.4.2).

Table 2: Specification of ABS *Terluran 958I*® [32, 33]

Property	Test method	Value	
density	ISO 1183	1.05	$\frac{g}{cm^3}$
MVR(220°C, 10 kg)	ISO 1133	15	$\frac{g}{10min}$
Young's modulus	ISO 527-2	2 700	MPa
molding shrinkage		0.4–0.7	%
thermal conductivity	DIN 52612	0.17	$\frac{W}{m \cdot K}$
recommended drying temperature		80	°C
recommended drying time		2–4	h
recommended melt temperature		210–270	°C
recommended mold temperature		40–70	°C

3.1.4 *Processing parameters*

For the given studies process parameters besides those varied during the parameter studies were chosen to influence the sink mark formation as low as possible. In some preliminary tests, a process window was developed to cover the whole possible scope of process parameters. The cooling time was set high enough to avoid any influence on the resulting sink mark. The switch-over point was chosen at a moment where the mold was just not filled completely. The temperature profile of the barrel was departed in four parts, where each was set 5 °C higher than the previous one.
As there was no such sensor available, it was not able to measure the *melt temperature* directly. Because of this, the die temperature was used as a parameter instead. It is assumed that it has comparable influence on the formation of sink marks as the melt should have approximately die temperature when being injected.
The *mold temperature* itself varies strongly during an injection molding process. The resulting uncertainty makes it unusable for systematic parameter studies. It would be possible to use the mold temperature at a certain moment of the injection molding process as a parameter, such as the temperature at the beginning of the cycle. But as the actual mold temperature course depends on the other parameters, as on the die temperature, it would not be possible to keep it constant when other parameters are varied. To avoid this problem, the coolant temperature was used as a parameter instead, which stays constant. Nevertheless, the mold temperature was measured during the injection molding process. Depending on the other parameters it usually was 2 to 5 °C hotter than the coolant temperature. The tested parts were produced in constant processes in so far as the production process was repeated until the mold temperature curve was equal for at least three parts in series. Thereby, it was guaranteed that all the parts were produced at certain mold temperatures.

According to Table 2, material was dried for two to four hours at 80 °C before use. Both mold temperature and melt temperature were kept inside of the limits recommended in Table 2. The cycle time of this process was 31 s.

The main molding plan is given in Table 4. The idea was to increase the holding pressure in increments of 40 bar, the injection velocity in increments of 10 cm^3/s, and the die temperature in increments of 10 °C, each at constant other parameters. To save time, for holding pressures of 270 bar and 350 bar there were no specimens produced with injection velocities of 80 cm^3/s or 100 cm^3/s. Thereby, 4 out of 25 tests could be saved and the most important settings could be tested. For each adjustment five parts were produced in order to monitor process constancy.

To resolve the influences of holding pressure and injection velocity finer, one series of both holding pressures and injection velocities were produced, each at constant further parameters. Thereby, pressure was varied from 280 bar

Table 3: Chosen process parameters

Parameter	Value(s)	
holding pressure time	4	s
cooling time	20	s
switch-over point	screw at 49	cm^3
coolant temperature	40	°C
die temperature	230/240/250	°C
injection velocity	10, 70...110	$\frac{cm^3}{s}$
holding pressure	40, 230...390	bar

Table 4: The molding plan of the parts produced at a coolant temperature of 40 °C. There were five parts produced for each injection molding program. There were no parts produced with injection velocities of 80 cm^3/s or 100 cm^3/s for holding pressures of 270 bar and 350 bar to save time. Additionally to that, the injection molding program at a die temperature of 240 °C was repeated for a coolant temperature of 50 °C. Further, there were parts produced with lower increments of both holding pressure and injection velocity at constant other parameters.

$T_{die} \rightarrow$	230 °C					240 °C					250 °C				
$p_{hold} \rightarrow$ $\downarrow v_{inj.}$	230 bar	270 bar	310 bar	350 bar	390 bar	230 bar	270 bar	310 bar	350 bar	390 bar	230 bar	270 bar	310 bar	350 bar	390 bar
70 cm^3/s	•	•	•	•	•	•	•	•	•	•	•	•	•	•	•
80 cm^3/s	•		•		•	•		•		•	•		•		•
90 cm^3/s	•	•	•	•	•	•	•	•	•	•	•	•	•	•	•
100 cm^3/s	•		•		•	•		•		•	•		•		•
110 cm^3/s	•	•	•	•	•	•	•	•	•	•	•	•	•	•	•

to 410 bar in steps of 10 bar at an injection velocity of 90 cm^3/s and a die temperature of 240 °C (Section 4.1). Injection velocity was varied from 50 cm^3/s to 130 cm^3/s in steps of 10 cm^3/s at a holding pressure of 370 bar and a die temperature of 240 °C (Section 4.2).

Finally, to get information about the influence of the mold temperature, the molding plan was repeated for a coolant temperature of 50 °C at a die temperature of 240 °C (Section 4.5).

As variation of temperatures in injection molding takes considerable time, they were variated stepwise. Thereby, randomization could not be achieved. To avoid an influence of the molding sequence the molding process would have to be repeated. As the main aim of this work was the measurement methodology, the risks caused by missing randomization were considered to be acceptable.

Because of the large process window, the production process did not work without any problems. Depending on the injection molding parameters it happened that the gate was not demolded correctly and had to be demolded by hand. Thereby, process instabilities were induced as the mold temperature cycle could not be kept constant which partially could not be avoided. This happened for injection molding programs at the borders of the process window, as for low temperatures and low holding pressure at the same time. It may be that some of these parts produced with problematic injection molding parameters are produced with a slightly lower mold temperature due to these instabilities. Everything in the producer's power was done to minimize these instabilities. Nevertheless, it is possible that there is an influence on the sink mark formation on the appropriate specimens.

3.2 FORMATION OF SINK MARKS

According to Carley and Whittington, a sink mark is defined as

> "[...] shallow depression or dimple on the surface of an injection-molded article, usually in a thick section, caused by local internal shrinkage after the gate seals, or by a slightly short shot. [...]" [34]

Local internal shrinkage can be seen as a local variation in the volumetric shrinkage. Volumetric shrinkage starts during solidification and lasts until the part's temperature is constant which may take time after a part's ejection [35]. Sink marks usually occur at areas of significant local change in wall thickness, as ribs, bosses or undercuts [36]. Because of the higher amount of plastic mass to be cooled down in an area with increased section thickness, this area is called an area of increased *thermal mass* [31]. In Figure 8 the effect of rib and wall thickness on the formation of sink marks is illustrated.

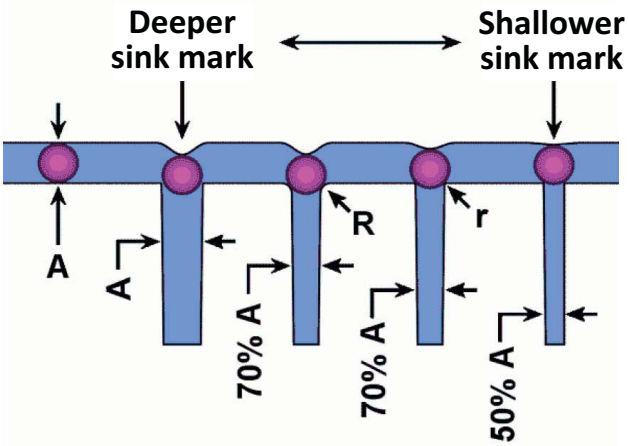

Figure 8: Formation of sink marks. The diameters of the little spheres are equal to the part's wall thickness A. Volumes in the part's wall with diameters bigger than A produce sink marks. The depth of the sink mark depends on the ratio of the rib's thickness to the one of the wall as well as on the radii of curvature. [14]

Sink marks themselves do not affect a part's mechanical properties in most cases, but they make it look of lower quality. In fact, as high-quality industry tries to avoid sink marks, they have become an indicator for a cheap production[1].
Prevention of sink marks itself sometimes produces more failure than it prevents, if it goes along with strong internal stresses. For example, very fast cooling of the outer area of an injection molding part can prevent sink marks, but vacuoles can be produced.

In this work, only the visual appearance of sink marks is of interest. To avoid sink marks, it is necessary to do diligent construction work and to

1 Even though sink marks are sometimes not of interest, they cannot be overlooked as they indicate a build up of internal stresses. [31]

beware of non-uniform thermal mass. As injection molding parts have to fulfill a lot of specifications, it is not possible to completely avoid sink marks in most cases. For example, ribs and gussets strengthen part geometry and thereby they are not abdicable. In those cases it may be necessary to implement an inspection system that quantifies the visibility of the defect.

According to Hayden, the visibility of a sink mark depends on the part's surface texture, its color as well as depth and width of the sink mark. Sink marks seem to be deeper if they are deeper or wider, or if the surface is brighter or less textured, where depth is far most influential. Sink marks shallower then 5 µm seem to be invisible as a rough rule of thumb. Texture depths greater than three times the depth of the sink mark are required to conceal sink marks (on black surfaces). [14, 15]

As the parts investigated in this work were produced with a given material and a given tool, the influence of machine settings on sink mark occurrence was of interest. Generally, possible influential machine parameters are melt temperature, mold temperature, coolant temperature, cooling time, holding time, fill time, injection rate, cavity pressure and holding pressure. [31, 37]

Mathivanan and Parthasarathy found out that the most influential processing parameters (i.e. for a given tool and material) are melt temperature, mold temperature and holding pressure, followed by holding time, velocity-pressure-switch over and injection time. For their studies they simulated an injection molding process using the data of a Cycolac AR® ABS Co-Polymer and compared the results to the ones of some other kinds of polymers. To reduce sink marks, they advise to increase melt temperature, to increase holding pressure and to lessen mold temperature [18, 38]. This is a contradiction to Whittington's dictionary of plastics, which advises to reduce both melt and mold temperature. [34]

Also, Ye and Leopold come to the conclusion that higher melt temperature produces sink marks due to the higher shrinkage. They used various materials for their research, where one of them was ABS. [15, 39]

Malloy found that sink mark appearance can be reduced by positioning of cooling lines in areas where the part is thicker. Thereby, the formation of sink marks in these regions could be reduced. However, while mold temperature was found to have an influence on the formation of sink marks, melt temperature was more influential. [40]

Part design and tooling have important influences on formation of sink marks. Although different designs are not compared in this work, one have to be aware of its effects. Mathivanan and Parthasarathy figured out that a sink mark's distance from the gate is far the most influential value. It is much more influential than temperatures or holding pressure. Rib/wall-ratio is an-

other important factor. [18]

Liou et al. studied both geometrical and processing parameters on the formation of sink marks. They found that the packing pressure was the most influential processing parameter, where rib thickness was the most effective design variable. Melt and mold temperature were found to be also highly influential, such as fillet radius. [41]

Shen et al. combined numerical simulation with Taguchi design-of-experiment technique to investigate the influence of process conditions and cavity geometry on sink marks of injection molded parts and optimize process conditions and cavity geometry. They found part thickness, holding pressure, melt temperature and mold temperature to be the most important factors. [42]

Tursi and Bistany recommended to use low temperatures, high dwell times and high holding pressures to reduce sink depth or to position ribs closer to the gate and perpendicular to the flow direction. [43]

Wang et al. found boss thickness and melt temperature to be the most important factors on formation of sink marks. [44]

Of course, also material has influence on sink mark appearance. Tursi and Bistany measured that semi-crystalline PP developed sink marks four times deeper then amorphous ASA [43] because of the increased shrinkage for semi-crystalline polymers. As mentioned in Section 3.1.3, ABS is the usually chosen polymer for measurement of sink marks [31]. This may be because of the prevalent use of ABS in high quality industry.

Overall, the mechanism of sink mark formation and the influencing factors have not yet been conclusively clarified. It seems as if some of the authors investigated sink marks only beside a couple of other injection molding defects and did not pay sufficient attention to them. Others seem to investigate sink marks in detail in their work but to pay more attention to the influence of the design and the material than to the one of processing parameters. Hence, in some works the formation of sink marks plays only a secondary role and some of them spend more time on the influence of the other influencing factors than on the one of the processing parameters. Additionally, there are many authors who do not make sufficient comments about their used material. This may be reasons why several researchers contradict each other and deliver partially different results.

3.3 IMAGE ACQUISITION FOR THE MEASUREMENTS

For image acquisition, a *Stingray F-504 5-megapixel camera* by *Allied Vision Technologies* was used. It was controlled directly by MATLAB® via an *IEEE 1394 interface* cable. Images were acquired using a *C2514-M(KP) lens* by *Pentax Corporation* with 25 mm focal length. [45]

The light source was an *vicolux® FAL11-W* LED array with an overall area of 240×180 mm² and a power of 35 W. In a working distance of 100 mm, its maximum illumination is 12 500 lx [46]. It was equipped with a diffuser to achieve uniform light emission. An aperture was used in order to direct a specific light pattern onto the surface. Prior image acquisition, the light source was on for at least 60 minutes to guarantee brightness stability[2].

In image processing the part of an image where the observed detail occurs (in this case the sink mark) is called *region of interest*. In this case, the region of interest was about 5 times 5 mm² in size. The system was calibrated to this region.

In preliminary tests it was found out that sink marks are most apparitional when viewed in almost *specular angle*[3], which is observable when watching people while they are evaluating the sink mark. Humans try to inspect the object in a manner that ensures light reflection in a specular angle all by themselves.

The optimal specular angle depends on the depth of the sink mark. Too steep angles do not produce shadows whereby sink marks are not visible. Too flat ones cause too low grayscale graduation. That is to say sink marks are not differentiated. The chosen angle of 65° (Figure 9, Table 5) produces best differences for medium strong sink marks.

Similarly, the width of the aperture correlates with the expected strength of the sink mark. The wider the aperture, the more distinguishable strong sink marks (until a certain width) are. The chosen width of 3.5 cm induced an emitting area of 84 cm².

In order to avoid overexposure and blooming effects it was assured that light did not illuminate the sensor of the camera directly.
All important setup preferences are given in Table 5. Mind that the application was two-dimensional in that all angles normal to image plane in Figure 9 were set to 0°. Camera angles were set with an error of about 0.2°, angles of light source with an error of about 2°, whereas it was exposed that

2 It was measured in a preliminary test that the light source was reliably constant after 60 minutes.

3 Specular angle was defined by Ingersoll as reflection of light in the angle of incident light [47]. In this work, the reflection was not completely specular, as the camera was slightly shifted (for the setup parameters see Table 5).

the process is quite robust in spite of these errors as long as the angle of light reflection stays constant. To achieve this, the angles were set first, and afterwards calibration of distances balanced the setup. As distances were set in a manner that the sink mark was central in the picture and medium illuminated it may occur that they vary quite strong without effecting the results critically. The errors in angles seem to be relatively high, but as long as the setup is not altered amongst the measurements the errors have considerably low influence on the inspection results since the diffuser guarantees diffuse illumination. Nevertheless, the results are only comparable to each other as long as the calibration does not have to be redone in between. Consequently, in this work results are compared to each other only if they were inspected using one and the same calibration.

The major problem was to position the specimens in the specimen holder. Since different processing parameters result in different warpage, specimens did not always fit in the rack exactly. The developed methodology is sensitive to angle variations. To minimize this problem, positioning of the specimens had to be done very warily.

Image file format was set to lossless 12-bit RAW with a resolution of $2\,452 \times 2\,056$ pixels[4] and was converted to true color RGB-matrix format by MATLAB®'s function `demosaic` [48].

Focussing was done manually by using focus assisting tools once and was not altered afterwards to achieve constant conditions. Equally, gain, color balance, shutter speed and sharpness correction were set manually (Table 5).

As the optimal angle of illumination is dependent on how strong the sink mark is, it is considered to install an appliance to vary the angle of the specimen during measurement in the future to take more than one picture per specimen. Thereby, the process would take a lot more time but would further increase measurement preciseness for extreme borders of sink mark occurrence. That has to be considered together with process speed and shot rates.

In an industrial application it is suggested to further improve the calibration for the expected visibility of the sink mark to minimize errors and to automate the positioning of the specimen which is the major source of measurement errors. This could be done in the course of the adjustment of a robotic handling system. In doing this, it should be possible to abandon the elimination of measurement outliers.

4 This relatively high resolution would not be needed. It would suffice to acquire the images with less resolution, resulting in an accelerated process time. Equally, it is not strictly necessary to use that high bit depth of 12 bits. Due to the good contrast of images, a bit depth of 8 bits seems to be sufficient. Thereby, the process of image acquisition could be accelerated. To avoid doubts in the given work's results it was decided to use this high resolution nevertheless.

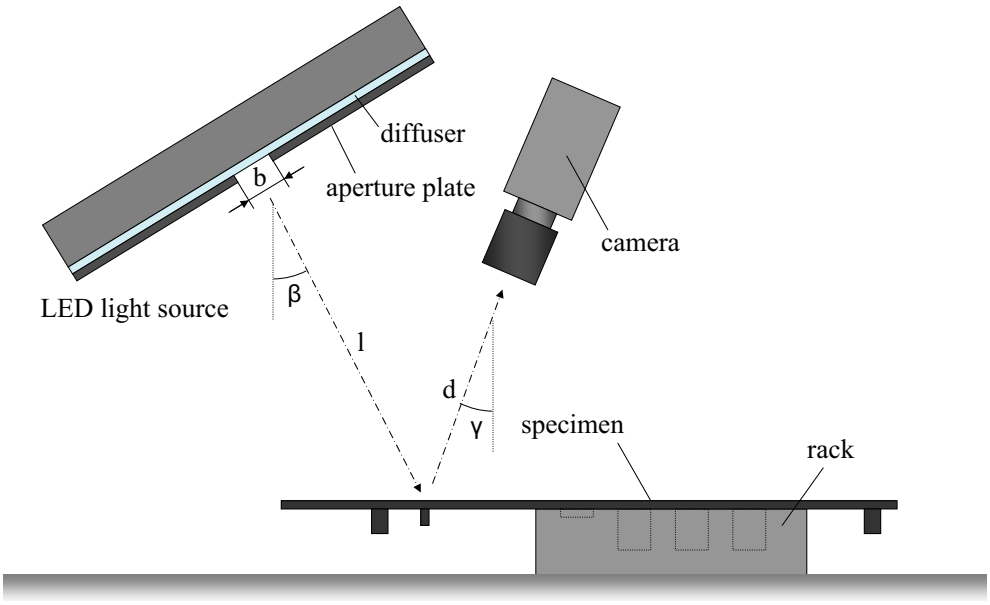

Figure 9: Principle of the photographic measurement setup

Table 5: Parameters of image acquisition (cf. Figure 9)

	Parameter	Value	
	sharpness correction	0	
	shutter speed	2 300	trigger units
	white balance	[391, 530]	a.u.
	gain	0	
d	surface point to camera sensor	135	mm
l	light source to surface point	235	mm
β	illumination direction to the vertical	25°	
γ	optical axis to the vertical	20°	
b	aperture	35	mm

This methodology was developed to measure only one sink mark at once. In industries, it might be necessary to measure several sink marks at the same time. For two different sink marks within a small surface area, this should be no issue as they can both be illuminated in specular angle at once. For sink marks that are not in line with each other further cameras are needed.

3.4 IMAGE PREPROCESSING

Preprocessing is needed to reduce noise and scratches prior to sink mark evaluation. The software used for calculations and visualization of results was
MATLAB®, version R2009b (The MathWorks, Inc.). Thereby, mainly the Image Processing Toolbox was used.

The numeric preprocessing operations used to improve the image information are:

A. Converting the color images to luminance matrices (gray-scale images) (Section 2.1.2).

B. Defining the *region of interest*.

C. Reducing image size to accelerate calculations.

D. Spatial filtering to reduce noise, dust and scratches.

3.4.1 *Converting color images to luminance matrices*

The only information out of acquired images needed for this work is the luminance. To eliminate hue as well as saturation RGB images are converted to gray ones.

In MATLAB®'s Image Acquisition Toolbox, function `rgb2gray` automatically calculates the luminance of an image using [49]:

$$I = 0.2989R + 0.5870G + 0.1140B \tag{3.1}$$

For an explanation of this formula, go to Section 2.1.2. As specimens were gray and thus colors were distributed similarly, there was no significant difference between the different options to calculate lumination. For this work, function `rgb2gray` was chosen.
Since the three values R, G and B were reduced to just one there was no dimension of the color any more. Hence, there were only two matrix dimensions remaining resulting in a lot more flexibility for the further processes.

In order to avoid rescaling and gray scale conversion of images it should be considered to use a gray scale camera with lower resolution for the industrial application.

3.4.2 *Definition of the region of interest*

The system had to be calibrated once to the region of interest. Therefore a script was implemented that allows an operator to define the center of the sink mark and its size in pixels (Figure 10) [50]. The region of interest was about 300 to 400 pixels in both directions. A size of 400 pixels seemed to be a good choice for all investigated sink marks and as long as the setup was not altered, it did not have to be recalibrated.

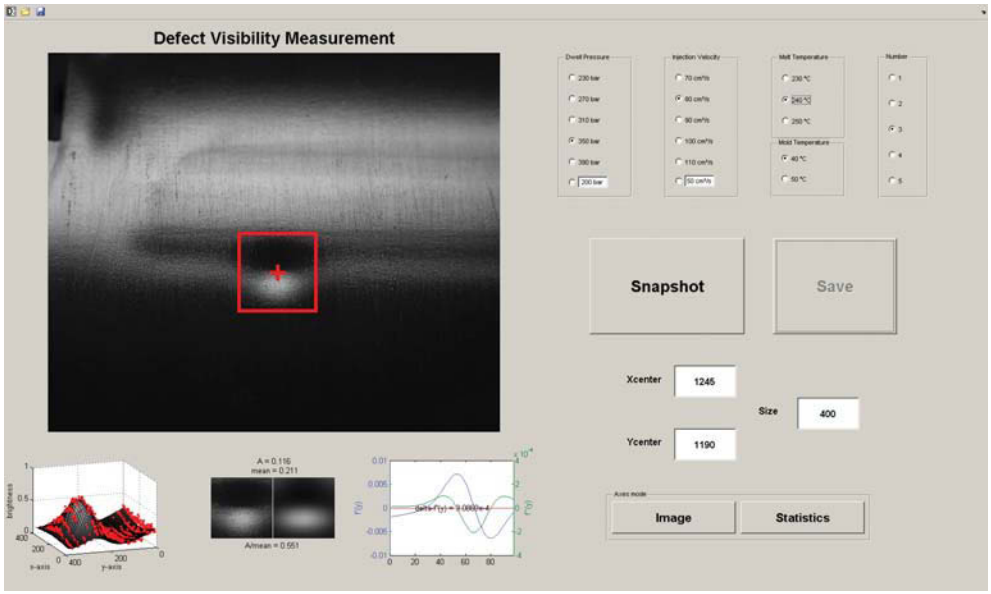

Figure 10: The implemented calibration script to locate the region of interest [50]. Upper left is the acquired image. The red square denotes the region of interest. It can be calibrated individually for the sink mark's size and location. By clicking "Snapshot", an image is acquired and evaluated automatically. Calculation results are expressed underneath the acquired image. By clicking "Save" the image and the corresponding results are saved together with the given properties.

3.4.3 *Spatial filtering and size reduction*

Next two steps are filtering and size reduction. The image is to be filtered to avoid an influence of high-frequency image phenomena. Based on preliminary studies an average filter was found to be an appropriate choice for the given case.
Afterwards, the size of the image had to be reduced. As mentioned in Section 3.3, the resolution of the images was very high to avoid doubts in the given work's results. Since fitting calculation time is strongly dependent on the image size, a lot of time can be saved thereby. Thus, some high-frequent information in the image is lost. As following calculations are based on low-frequent information the loss of important information is rather low.
Since size reduction works by calculating the means of congruent regions, the average filtering is included automatically, whereby some additional cal-

culation time was saved. The formula for size reduction from a side length of m to a side length of n pixels is:

$$g(x,y) = \frac{\sum_{i=1}^{d}\sum_{j=1}^{d} f((x-1)d+i,(y-1)d+j)}{d^2} \tag{3.2}$$

where $d = \frac{m}{n}$. Thus, each pixel of g forms the mean of each corresponding pixel neighborhood of f. As pixels cannot be intersected, the indices of f have to be rounded to integers.

The side length of the downsized image was set to $n = 100$, regardless of the size of the sink mark in the image, which is a fast, convenient and exact way as long as the region of interest is defined correctly. The chosen size was chosen by taking into account both calculation time and loss of information (Section 3.5.4).

3.5 MODELING OF SINK MARKS

The intensities of the images' pixels were fitted to an analytic model based surface function. On the one hand this enables the evaluation of the sink mark by using its fit parameters on the other hand complex further processing as differentiation becomes possible thanks to the continuity of the function. The fitting was processed with the MATLAB® function `fit` of the Curve Fitting Toolbox [51].

The surface fit was performed because of the graded illumination of the specimens (caused by a graded distance of the light source over the region of interest) and the corresponding difficulties in finding the sink marks' exact extreme value positions. It was not possible to simply examine an illumination profile as it was the case in the work by Pacher [20]. The profile would always have to pass both the maximum and the minimum of the reflected intensity field of the sink mark. Therefore, those extreme values have to be found previously. There are MATLAB® functions `imregionalmax` and `imregionalmin` which facilitate the search for local extreme values [52, 53]. When these functions were used in preliminary tests it appeared that they need very smooth and undistorted data to provide reasonable results. Since the surface of the specimens was highly structured and scratched, performed calculations lead to a lot of errors and outliers. Additionally, the illumination decrease with distance from the light source had to be eliminated which could be achieved by fitting methods. This is why surface fitting seemed to be an adequate choice.

3.5.1 *Fit functions*

The coordinates were chosen that way that the y-coordinate ran from the top of an image to the bottom and the x-coordinate ran from left to right. That is to say, the y-coordinate conformed to the projection of the illumination vector on the surface of the specimen.

In a first attempt the shape of a sink mark at its center was approximated by a polynomial of degree 2 [54]. The borders of sink marks could not be described with this model. Instead, a *Gaussian curve* appeared to be more adequate for a better description of the contour of sink marks[5]. Additionally, the Gaussian curve is a simple and easily differentiable function which is useful for further processing. Current topographical measurements on sink marks confirm that a Gaussian curve is a good approximation for the physical shape of sink marks [55].

When surfaces reflect light with a given direction of incidence **i**, the intensity of the reflected light detected by a camera depends on the relation between the direction of specular reflection **s** and the optical axis of the camera **c** (Figure 11). The more these vectors coincide, the brighter the reflection captured by the camera is. The optical axis of the camera **c** was assumed to be parallel for all positions on the sink mark as the camera to surface distance was big compared to the dimensions of the region of interest. The direction **s** depends on the normal vector **n** of the reflecting surface at a given position on the surface. In other words, the measured intensity at each point of the viewed sink mark depends on the surface's tangent **t**. As a function's tangent conforms to its first derivative the intensity of the reflected light is expected to be proportional to the surface's derivative (in the direction parallel to the projection of the light incidence **i** on the surface). Hence, in this case the illumination is expected to correlate with the first derivative in one direction of a Gaussian surface.

Due to the formation of shades, the dark areas in the images of deep sink marks were bigger than the bright ones. This led to imprecise fitting. Especially for very strong sink marks, the size differences between the bright and the dark areas were considerable. To solve this problem, the Gaussian curve in the illumination direction was replaced with a *skew normal distribution* function. The first derivative of this function looks similar to the one of the Gaussian curve, except that the maximum and the minimum are not symmetric in height and width (cf. Figure 12). Apparently this function models the images of sink marks better.

In a nutshell, a sufficient function to fit the intensity function of the sink marks was the *first derivative of a skew normal distribution* in y-direction, ex-

5 Since the first terms of the Taylor expansion of the Gaussian curve conform to a polynomial of degree 2, the assumption that a Gaussian surface could describe the sink mark well seemed to be proximate.

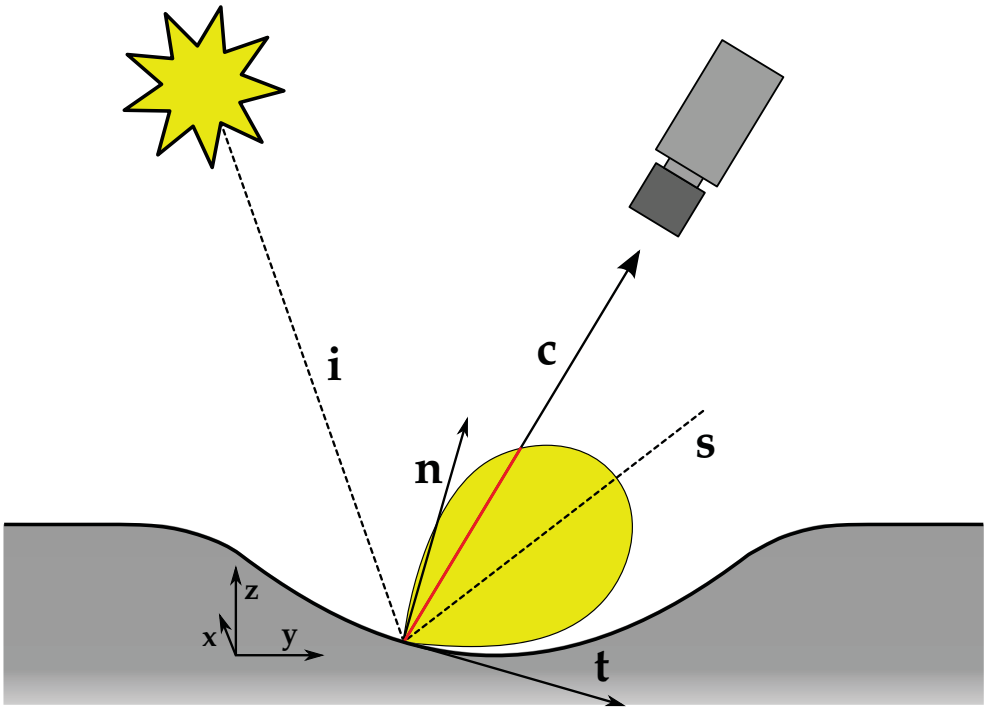

Figure 11: The reflection of light with the direction of incidence **i** on a surface. The intensity of the reflected light captured by the camera highly depends on the relation between the direction of specular reflection **s** and the optical axis of the camera **c**. The direction of **s** depends on the normal vector **n** or on the tangent **t** of the reflecting surface, respectively.

panded to 2D by multiplying with an unskewed *Gaussian curve* perpendicular to it (x-direction)[6].

The Gaussian curve is defined by [56]

$$g(x) = \frac{1}{\sigma\sqrt{2\pi}} \exp\left[-\frac{1}{2}\left(\frac{x-\xi}{\sigma}\right)^2\right] \tag{3.3}$$

where ξ denotes the position of the maximum and σ denotes the standard deviation of the Gaussian curve in $g(x)$.

According to Azzalini and Dalla Valle, the skew normal distribution $s(z)$ with skewness parameter α is defined by

$$s(z) = 2 \cdot \phi(z) \cdot \Phi(\alpha z) \tag{3.4}$$

where ϕ denotes the *probability density function* of the normal density function

$$\phi(z) = \frac{1}{\sqrt{2\pi}} e^{-\frac{z^2}{2}} \tag{3.5}$$

6 It was assumed that the x- and y-direction were independent on each other, allowing partial differentiation. This relates to a neglect of the *correlation* between x and y, which is possible as illuminance was parallel to y-direction, and it leads to a reduction of calculation time and a gain in process stability.

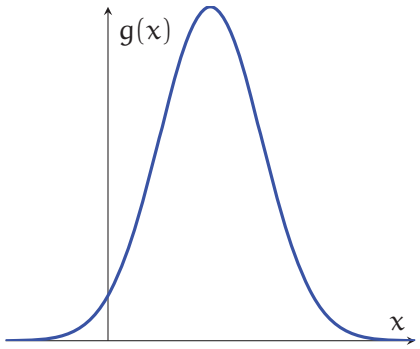

(a) Gaussian curve $g(x)$ with $\xi = 1$ and $\sigma = 0.5$

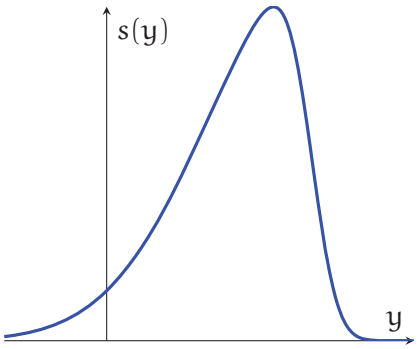

(b) Skew normal distribution $s(y)$ with $\gamma = 2$, $\omega = 1.0$ and $\alpha = -5$

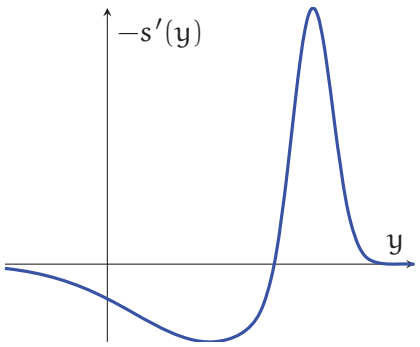

(c) Negative derivative $-s'(y)$

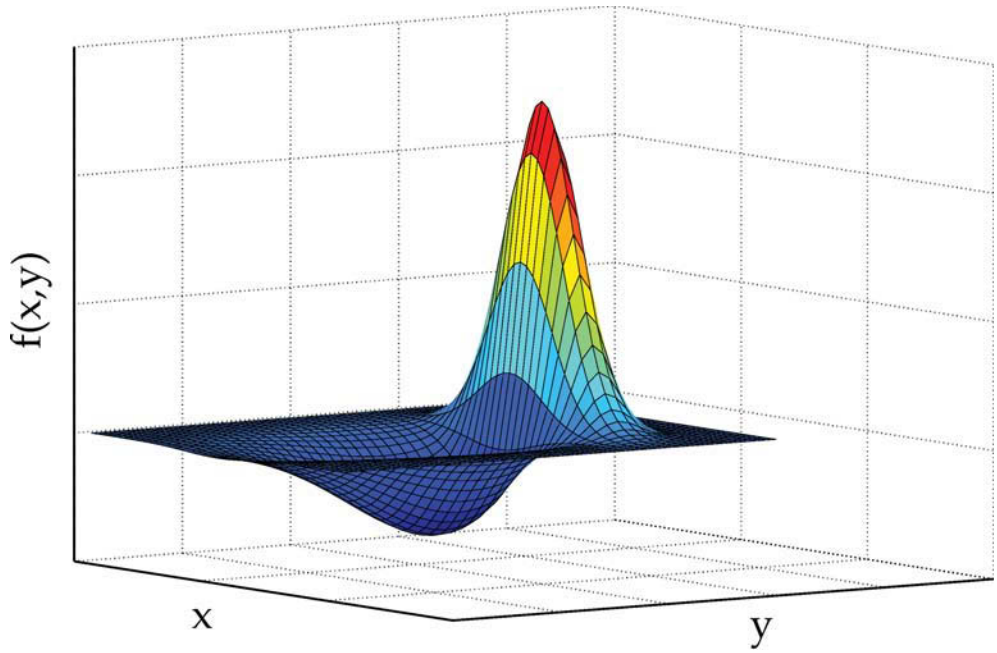

(d) Surface fit function $f_1(x, y) = g(x) \cdot s'(y)$

Figure 12: 3D-graph of the model function (see also Section 3.5.1). The surface function (d) is the product of the curves (a) and (c). It approximates the intensity function of the image of a sink mark.

and Φ denotes its *cumulative distribution function* [57]:

$$\Phi(z) = \int_{-\infty}^{z} \phi(t)dt = \frac{1}{2}\left(1 + \operatorname{erf}\left(\frac{z}{\sqrt{2}}\right)\right) \tag{3.6}$$

The *error-function* erf that appears in Equation 3.6 is defined by [58]:

$$\operatorname{erf}(z) = \frac{2}{\sqrt{\pi}} \int_{0}^{z} e^{-t^2} dt \tag{3.7}$$

The chosen function has to be variable in its size to be able to fit differently perceptible sink marks. Equally it must be variable in its position, so that the center of the sink mark does not necessarily have to be in the center of the image. By adding position γ and scale ω by $z = \frac{y-\gamma}{\omega}$, Equation 3.4 becomes:

$$s(y) = \frac{2}{\omega} \cdot \phi\left(\frac{y-\gamma}{\omega}\right) \cdot \Phi\left(\alpha\frac{y-\gamma}{\omega}\right) \tag{3.8}$$

By using Equation 3.5 and 3.6, Equation 3.8 results in:

$$s(y) = \frac{2}{\omega} \cdot \frac{1}{\sqrt{2\pi}} \cdot e^{-\frac{(y-\gamma)^2}{2\omega^2}} \cdot \frac{1}{2} \cdot \left[1 + \operatorname{erf}\left(\alpha\frac{y-\gamma}{\omega \cdot \sqrt{2}}\right)\right] \tag{3.9}$$

The graph of this function is displayed in Figure 12b. The differentiation of this equation with respect to y is given by:

$$\begin{aligned} s'(y) = {} & \frac{1}{\omega \cdot \sqrt{2\pi}} \cdot \left(-\frac{1}{2\omega^2}\right) \cdot 2(y-\gamma) \cdot \exp\left(-\frac{(y-\gamma)^2)}{2\omega^2}\right) \cdot \ldots \\ & \ldots \cdot \left[1 + \operatorname{erf}\left(\alpha\frac{y-\gamma}{\omega \cdot \sqrt{2}}\right)\right] + \frac{1}{\omega \cdot \sqrt{2\pi}} \cdot \ldots \\ & \ldots \cdot \exp\left(-\frac{(y-\gamma)^2}{2\omega^2}\right) \frac{d}{dy}\left[\operatorname{erf}\left(\alpha\frac{y-\gamma}{\omega \cdot \sqrt{2}}\right)\right] \end{aligned} \tag{3.10}$$

The differentiation of the error-function according to Equation 3.7

$$\frac{d}{dy}\left[\operatorname{erf}\left(\alpha\frac{y-\gamma}{\omega \cdot \sqrt{2}}\right)\right] = \frac{2}{\sqrt{\pi}} \cdot \frac{d}{dy} \int_{0}^{\alpha\frac{y-\gamma}{\omega\sqrt{2}}} e^{-\tau^2} d\tau \tag{3.11}$$

is performed by the *Leibniz integral rule* [59]:

$$\frac{d}{dt}\int_{\chi(t)}^{\varphi(t)} f(\tilde{x},t)d\tilde{x} = \int_{\chi(t)}^{\varphi(t)} \frac{\partial}{\partial t} f(\tilde{x},t)d\tilde{x} + f(\varphi(t),t)\cdot\frac{d}{dt}\varphi(t) - \ldots$$
$$\ldots - f(\chi(t),t)\cdot\frac{d}{dt}\chi(t) \tag{3.12}$$

In this case, $t = y$, $\varphi(t) = \alpha\frac{y-\gamma}{\omega\sqrt{2}}$, $\chi(t) = 0$, $\tilde{x} = \tau$ and $f(\tilde{x},t) = e^{-\tau^2}$:

$$\Rightarrow \frac{2}{\sqrt{\pi}}\frac{d}{dy}\int_0^{\alpha\frac{y-\gamma}{\omega\sqrt{2}}} e^{-\tau^2}\cdot d\tau = \frac{2}{\sqrt{\pi}}\int_0^{\alpha\frac{y-\gamma}{\omega\sqrt{2}}} \overbrace{\frac{\partial}{\partial y}e^{-\tau^2}}^{0}\cdot d\tau + \ldots$$
$$\ldots + \frac{2}{\sqrt{\pi}}\exp\left[-\left(\alpha\frac{y-\gamma}{\omega\sqrt{2}}\right)^2\right]\cdot\frac{d}{dy}\left(\alpha\frac{y-\gamma}{\omega\sqrt{2}}\right) - 0 =$$
$$= \frac{2}{\sqrt{\pi}}\cdot\exp\left[-\left(\alpha\frac{y-\gamma}{\omega\sqrt{2}}\right)^2\right]\cdot\frac{\alpha}{\omega\sqrt{2}} \tag{3.13}$$

Using Equation 3.11 and 3.13, Equation 3.10 results in:

$$s'(y) = -\frac{y-\gamma}{\omega^3\cdot\sqrt{2\pi}}\cdot\exp\left[-\frac{(y-\gamma)^2}{2\omega^2}\right]\cdot\left[1+\operatorname{erf}\left(\alpha\frac{y-\gamma}{\omega\sqrt{2}}\right)\right] + \ldots$$
$$\ldots + \frac{\alpha}{\omega^2\cdot\pi}\cdot\exp\left[-(1+\alpha^2)\cdot\frac{(y-\gamma)^2}{2\omega^2}\right] \tag{3.14}$$

The graph of this function is shown in Figure 12c. In order to get a 2D-model function Equation 3.14 in multiplied by a Gaussian curve in x-direction. Combination of Equation 3.3 and Equation 3.14 by $f_1(x,y) = g(x)\cdot s'(y)$ gives:

$$f_1(x,y) = -\frac{1}{\sigma\sqrt{2\pi}}\exp\left[-\frac{(x-\xi)^2}{2\sigma^2} - \frac{(y-\gamma)^2}{2\omega^2}\right]\left\{\frac{y-\gamma}{\omega^3\sqrt{2\pi}}\cdot\ldots\right.$$
$$\left.\ldots\cdot\left[1+\operatorname{erf}\left(\alpha\frac{y-\gamma}{\omega\sqrt{2}}\right)\right] - \frac{\alpha}{\omega^2\pi}\exp\left[-\alpha^2\frac{(y-\gamma)^2}{2\omega^2}\right]\right\} \tag{3.15}$$

The function, that is to say, the model that was used to fit the surface reflected intensity is shown in Figure 12d. Creating the new variable $A = -\frac{1}{\sigma\omega^2\pi}$ simplifies the equation and has the positive side-effect that the scale ω of the function does not affect the function's size.

With increasing distance to the light source the intensity of the illumination decreased along the y-axis in the images. This affects the measurement

results since it influences the intensity function of the images to a higher degree than the sink mark does. It was corrected by adding a second degree polynomial with the coefficients C_0, C_1 and C_2 and the position C_{zero}. Equation 3.15 with $f(x,y) = f_1(x,y) + C_2(y - C_{zero})^2 + C_1(y - C_{zero}) + C_0$ leads to:

$$\begin{aligned} f(x,y) = A \cdot \exp\left[-\frac{(x-\xi)^2}{2\sigma^2} - \frac{(y-\gamma)^2}{2\omega^2}\right] \left\{\sqrt{\frac{\pi}{2}} \cdot \frac{y-\gamma}{\omega} \cdot \ldots \right. \\ \ldots \cdot \left[1 + \operatorname{erf}\left(\alpha \frac{y-\gamma}{\omega\sqrt{2}}\right)\right] - \alpha \cdot \exp\left[-\alpha^2 \frac{(y-\gamma)^2}{2\omega^2}\right] \Big\} + \ldots \\ \left. \ldots + C_2(y - C_{zero})^2 + C_1(y - C_{zero}) + C_0 \right. \end{aligned} \tag{3.16}$$

Equation 3.16 gives the implemented fit function. All nine fit parameters, including their initial values and their limits, are listed in Table 6.

3.5.2 *Fit parameters*

In a lot of test runs, the empirical fit parameters given in Table 6 turned out to be a good tradeoff between universality and robustness of the measurements. The main purpose of the chosen limits is to prevent the fitting process from diverging during the first iteration steps.

Table 6: Empirically found fit parameters with initial values and limits. $g(x)$ denotes the Gaussian curve in x-direction, $s(y)$ denotes the skew normal distribution in y-direction, $\mathbf{I}(x,y)$ is the image matrix to fit, and l is the side length of $\mathbf{I}(x,y)$.

	Parameter	lower limit	initial value	upper limit
A	amplitude	-50	0.1	50
ξ	position of $g(x)$	$\frac{1}{4} \cdot l$	$\frac{1}{2} \cdot l$	$\frac{3}{4} \cdot l$
σ	standard deviation of $g(x)$	10	100	1 000
γ	position of $s(y)$	$\frac{1}{4} \cdot l$	$\frac{1}{2} \cdot l$	$\frac{3}{4} \cdot l$
ω	standard deviation of $s(y)$	10	100	1 000
α	skewness of $s(y)$	-10	-5	10
C_2	correction term 2^{nd} degree	-0.01	0	0.01
C_1	correction term 1^{st} degree	-0.01	0	0.01
C_0	basic luminance	0	$\langle \mathbf{I}(x,y) \rangle$	1.2
C_{zero}	position of correction term	0	$\frac{1}{2} \cdot l$	l

Because of the high number of fitting parameters the fitting process would be highly unstable without proper limits. Especially the parameters C_2 and

C_1 had to be limited very rigidly. Otherwise, the polynomial would overcome the actual fit function of the sink mark preventing the detection and analysis of the sink mark.

3.5.3 *Results of the surface fitting process*

In Figure 13, an example of a fit surface in comparison to the input data is given. The calculated surface fit functions, re-converted to images, looked very similar to the images they were fitted to, as can be seen in Figure 14.

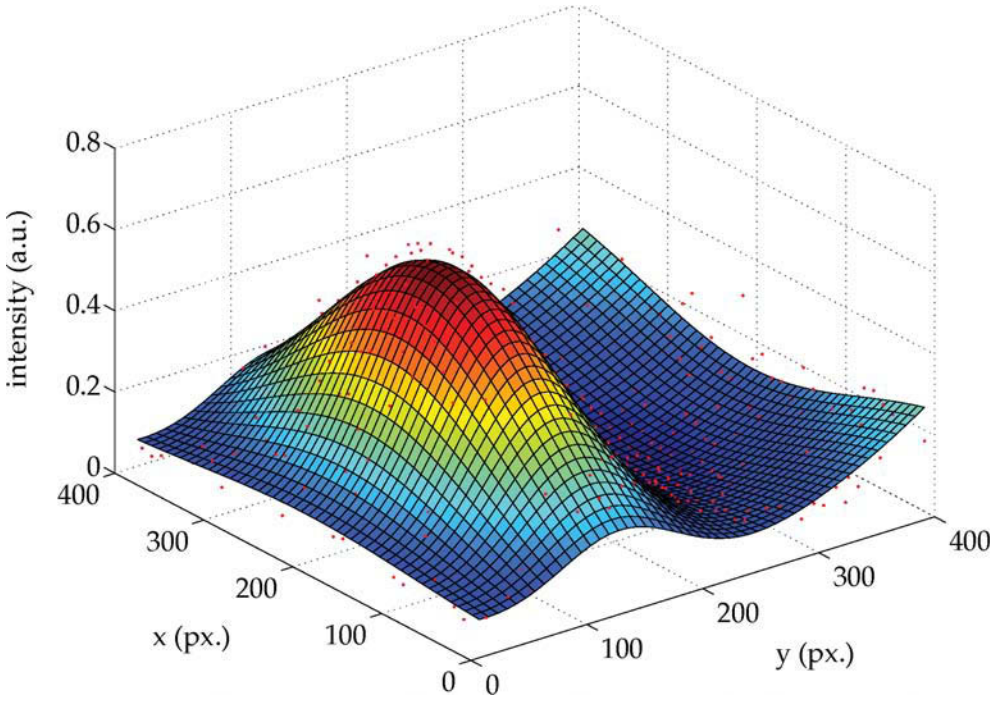

Figure 13: Example of a fit surface. The red dots denote the raw input data and the surface plot denotes the fitted function.

3.5.4 *Optimization of processing time*

For the application of the method in an assembly line it is necessary to reduce processing time as far as possible without corrupting the results considerably. At least, it should take shorter than the cycle time of the injection molding process[7]. The most time-consuming processes are the image acquisition process and the fitting process. The image acquisition process can be accelerated by using brighter illumination, whereby duration of exposure can be reduced. The fitting process time is mainly dependent on the size of the image to fit and the speed of the central processing unit of the used computer.
In a preliminary test, it was measured that the fitting time t_{fit} is approxi-

7 In high-quality industry, cycle times lower than ten seconds are rare.

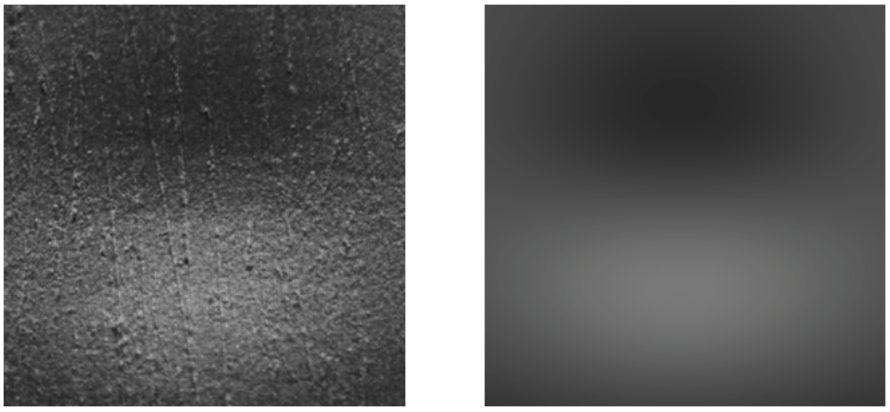

(a) (b)

Figure 14: A comparison of an original image (a) and the corresponding fitted image (b).

mately proportional to the number of pixels to fit, or to the square of the side length n of the image to fit:

$$t_{fit} \in \mathcal{O}(n^2) \tag{3.17}$$

As expected, the measurement errors decreased with higher pixel count. Of course, any omitting of pixels has an influence on the results, but for side lengths of 100 pixels and higher the relative error was found to be quite small (cf. Figure 15). As the side length must not be altered after calibration, this should not affect the results of the inspection critically. For this work, a side length of $n = 100$ (25 % of the original side length of the cropped region of interest) was chosen as it accelerated the process without causing considerable process impreciseness.

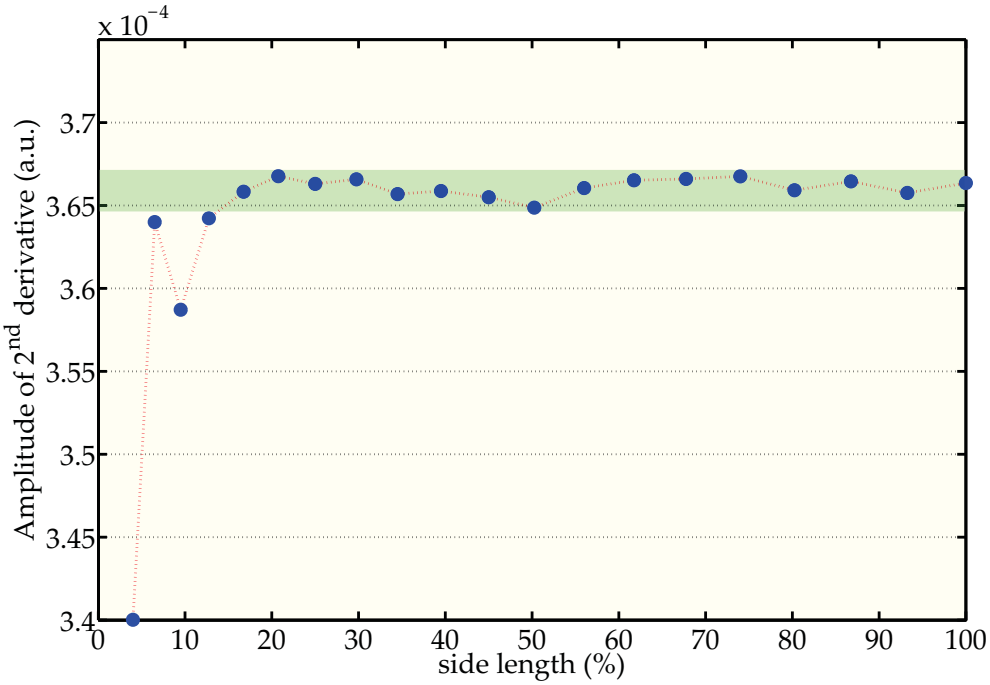

Figure 15: ASD in dependence on the side length of the image. A reduction to 15 % of the original side length does not considerably alter the results.

3.6 CALCULATION OF THE PERCEPTIBILITY OF SINK MARKS

3.6.1 *Handling of plain results*

As one would expect in images where no sink mark is visible the fitting process produces random indications. The standard deviations are significantly higher than otherwise, providing a condition parameter for the detection threshold for the sink marks. The surface fit delivers the standard deviations in both coordinate directions x and y in a direct way. It was found that if no sink mark was detected by the algorithm, these standard deviations were significantly higher. So, if one or both of these parameters were higher than five times the side length of the (downsized[8]) image, the condition parameter for evaluation of the sink marks' visibility was set to zero. In this case, the side length of the downsized images was 100 pixels. So the condition parameters of surfaces with one standard deviation higher than 500 pixels were set to zero.

3.6.2 *Calculation of the amplitude of the second derivative (ASD)*

In addition to the detection of sink marks, the quantitative evaluation of their visibility was a major task in this work. So, a parameter for the visibility of a sink mark had to be chosen. According to Gruber and Pacher, the amplitude

8 As explained in Section 3.4.3, the original images were unnecessarily big, resulting in high process times for which reason their size was reduced.

of the second derivative (ASD) is a useful parameter [19, 20]. In several tests, this parameter was compared with others, as for example the ratio of the amplitude to the mean of the image. In tests, ASD emerged to be a reliable and robust model parameter with low statistical spread.

The second derivative in y-direction of the fitted surface $\frac{\partial^2 f}{\partial y^2}$ was calculated using MATLAB® function `differentiate` [60]. This function allows the calculation of the second derivative with respect to y out of calculated fit parameters, resulting in a further surface function. As the amplitude of this surface is to be found, the extreme values of this surface is calculated using MATLAB® functions `imregionalmax` and `imregionalmin` [52, 53]. These two functions need very smooth data to work reliably. After the data is approximated by a surface function this is not an issue any more. The conditional parameter was chosen to be the difference between the highest local maximum and the lowest local minimum.

There are always extreme values at the borders of the image, where the gradient is not zero. The mentioned MATLAB® functions count these extreme values as regional extreme values as there are no pixels in the neighborhood whose values are higher or lower, respectively (see Figure 16). Mathematically, these extreme values at the borders of the image are absolute extreme values but no local ones as the gradient is not zero. Thus, extreme values at the borders of the image were ignored in the calculation.

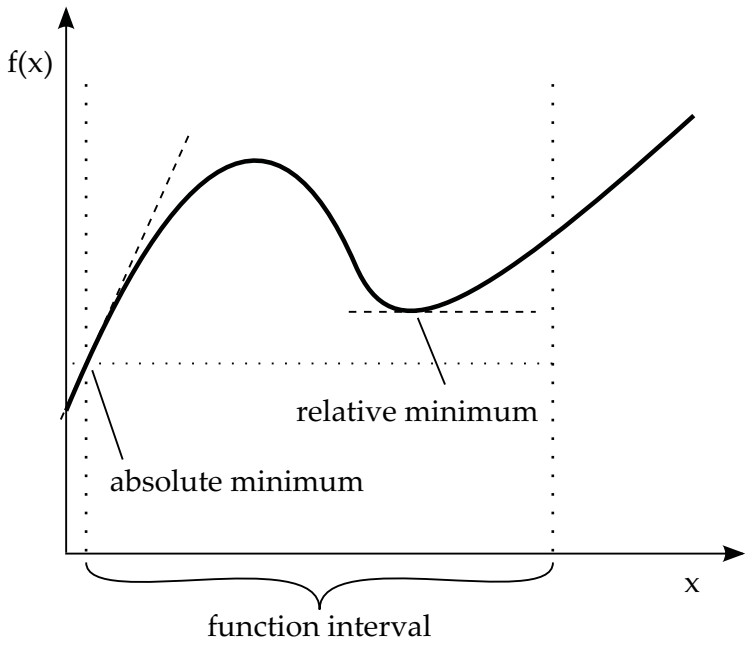

Figure 16: The absolute minimum at the border of a function interval is interpreted as a "regional extreme value" by MATLAB®'s function imregionalmin. Mathematically, it is no local minimum as the gradient is not zero. The relative minimum within the borders is the only local minimum from the mathematical point of view.

3.7 PROPERTIES OF THE DEVELOPED METHODOLOGY

The described method has a couple of advantages compared to the ones that were used so far [20]:

- One of the most important properties of this method is its potential to find the center of a local sink mark in an image. Previous methods, designed for linear sink marks, often work one-dimensional, whereby the problem of finding the sink mark is reduced to a simple extreme value problem. These algorithms fail as soon as they are applied to complex surfaces (extreme surface shape and structure deviations).
- Compared to previous methods, the method used in this work is a lot more sensitive. Even small distinctions of the perceptibility of different sink marks can be discerned. The mayor reason is the specular illumination which causes that the intensity of the light which is reflected into the camera highly depends on the shape of the specimen's surface. It is not necessary to define a threshold for the visibility as plain results can be identified only by their fit parameters. Thanks to this fact, it is possible to interpret if a sink mark is principally visible or not. This is a great advantage compared to previous methods.
- Thanks to the rough filtering and the surface fit, which lessen the influence of noise, the method is less sensitive to measurement errors that result from surface texture or noise. The methodology turned out to be quite robust while evaluating even unclean or damaged surface. Specimens where scratches or moisture cords occurred in the region of interest could be measured correctly. The surface defects did not affect the inspection results considerably.
- Due to the derivation of the illuminance, that excludes the influence of the mean brightness on the results, there is a comparative insensitivity to brightness fluctuations as long as the images are neither under- nor overexposed. The methodology turned out to be robust against influence caused by ambient light.
- The evaluated area can be chosen very small if necessary, allowing evaluation of sink marks near other surface defects, as it was the case in this work (cf. Figure 6 and Section 3.4.2).

Nevertheless, there are several limits to be considered:

- As most inspection systems the setup is sensitive to imprecise positioning and needs careful handling of the specimens. Due to the specular reflection already low misalignments of the measurements' settings can cause considerable luminance differences and subsequent measurement errors. This can happen by imprecise positioning and calibration of the setup or if parts are contorted due to the injection molding process. Nevertheless, strongly contorted parts may be discarded by using a preceding rough and fast process.

- It is necessary to calibrate the setup for the expected sink mark visibility. This calibration has an influence on the precision of the results. Once calibrated, the setup does not need to be altered anymore.
- Compared to some of the previous methods, this method requires longer processing time. This is due to the surface fit which is time-consuming. However, on the one hand the processing time is low enough for an application in an assembly line. On the other hand this period of time can be reduced significantly by stronger size reduction with only low loss in precision (cf. Section 3.4.3). In addition to that this drawback is continuously reduced by increasing computer performance.
- A drawback of this method is the fact, that with just one camera only the sink marks all along one line can be evaluated simultaneously. For more than two sink marks, where one is not in line with the others, either further camera units or further light sources are needed to achieve specular illumination.

4

MEASUREMENT RESULTS

In this section effects of process parameters on the formation of sink marks are investigated and compared to results in literature [18, 31, 34, 38–44]. For that reason specimens were produced at different process parameters. One dot-shaped sink mark on the surface of the specimens was selected for the measurements (cf. Section 3.1.2).

As mentioned in Section 3.1.4, two series of specimens with fine discretization of holding pressure and injection velocity were produced for better understanding of the dependency of sink mark formation on these two process parameters. In Section 4.1 and Section 4.2 the results of the measurements on both series are illustrated. In Section 4.3 the interrelation of the given two parameters is examined.

The next sections introduce the influence of the temperature on the perceptibility of the sink marks. In Section 4.4 the influence of the die temperature is presented. Especially the interrelation of the die temperature, the injection velocity and the holding pressure are examined. Section 4.5 presents the effects of the coolant temperature on the perceptibility of the sink marks.

In Section 4.6 the results of robustness tests are presented which give an estimate of the reliability of the new methodology.

4.1 INFLUENCE OF THE HOLDING PRESSURE ON THE PERCEPTIBILITY OF SINK MARKS

In a test series the holding pressure was increased from 280 bar to 410 bar in increments of 10 bar with five specimens for each pressure level, while the injection velocity was kept constant at 90 cm^3/s and the die temperature was at 240 °C. The results of the inspection of the sink marks are given in Figure 18. Some of the corresponding images are given in Figure 17.

In Figure 17 each row of the image array displays the sink marks of the five specimens produced at the same holding pressure level. The holding pressure used for production increases from top to bottom. The images within each row are from the same appointed process parameter. Small differences are caused by variations in the production process. The measuring points in Figure 18 each show the mean ASD value out of five measured specimens.

The threshold of perceptibility was assumed to be at about 390 bar holding pressure. Calibration was optimized for finer detection of shallow sink marks for these measurements to bring out the perceptibility threshold[1]. Thus the measurement's resolution is highest with small errors at the same time within the optimum range of values (area of calibrated light conditions).

As expected, an increase of the holding pressure reduces the formation of sink marks. Even under perfect illumination, sink marks formed on parts at a holding pressure of 390 bar are barely visible. Since only one sink mark of the series of the five specimens produced at 390 bar was detected, it is reasonable to assume the perceptibility threshold in this range of holding pressure.

It would be possible to detect such extremely shallow sink marks with a smaller aperture on the illumination device even better. Thereby, the perceptibility threshold of the methodology would be lowered while deeper sink marks would not be differentiated adequately any more (cf. Section 3.3). However, visual assessment has shown that these slight sink marks are barely visible for human eyes under normal conditions.

Comparison of the array of the sink marks in Figure 17 with the diagram in Figure 18 shows good correlation between the results of the methodology and the perceptibility of the sink marks. As emphasized in Figure 18, the threshold of perceptibility is at about 390 bar. Apparently, the lowest measurement errors are at ASD values below 1.5×10^{-4}, since the configuration of the test setup was calibrated for this substantive region close to the perceptibility threshold. In this range of values the variations of the measurements are very small whereas the variance of the measuring values increases for

1 As mentioned in Section 3.3, it is not possible to compare measurement results when the calibration was altered in between. To improve detection of deeper sink marks, the measurement calibration was optimized for deeper sink marks in the other measurements.

lower holding pressure levels.

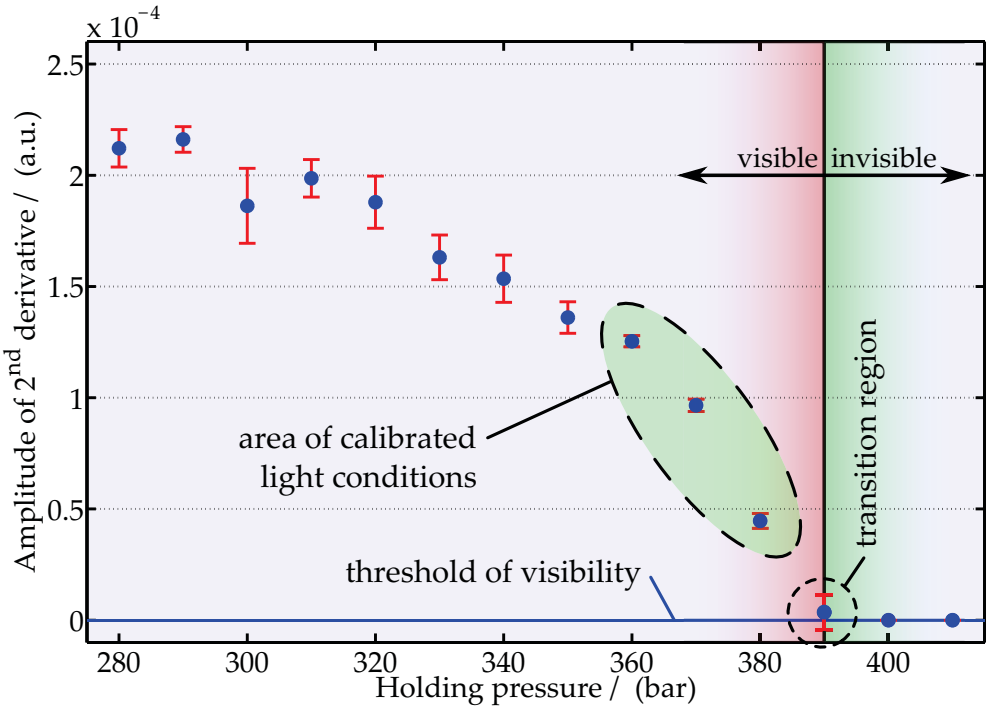

Figure 18: Measured ASD in dependence on the holding pressure. The die temperature and the injection velocity were kept constant at 240 °C and 90 cm^3/s, respectively (cf. Figure 17). The measuring points each show the mean ASD value out of five measured specimens. The holding pressure was increased for each series from 280 bar to 410 bar in increments of 10 bar. The fine resolution together with the high precision of the methodology is especially apparent for the pressure region the light conditions were calibrated for. For normal light conditions, the sink marks that are not detected by the methodology are below a human eye's threshold of visibility. To improve the detection of very shallow sink marks, as the one at 390 bar holding pressure in this example, it would be necessary to recalibrate the setup.

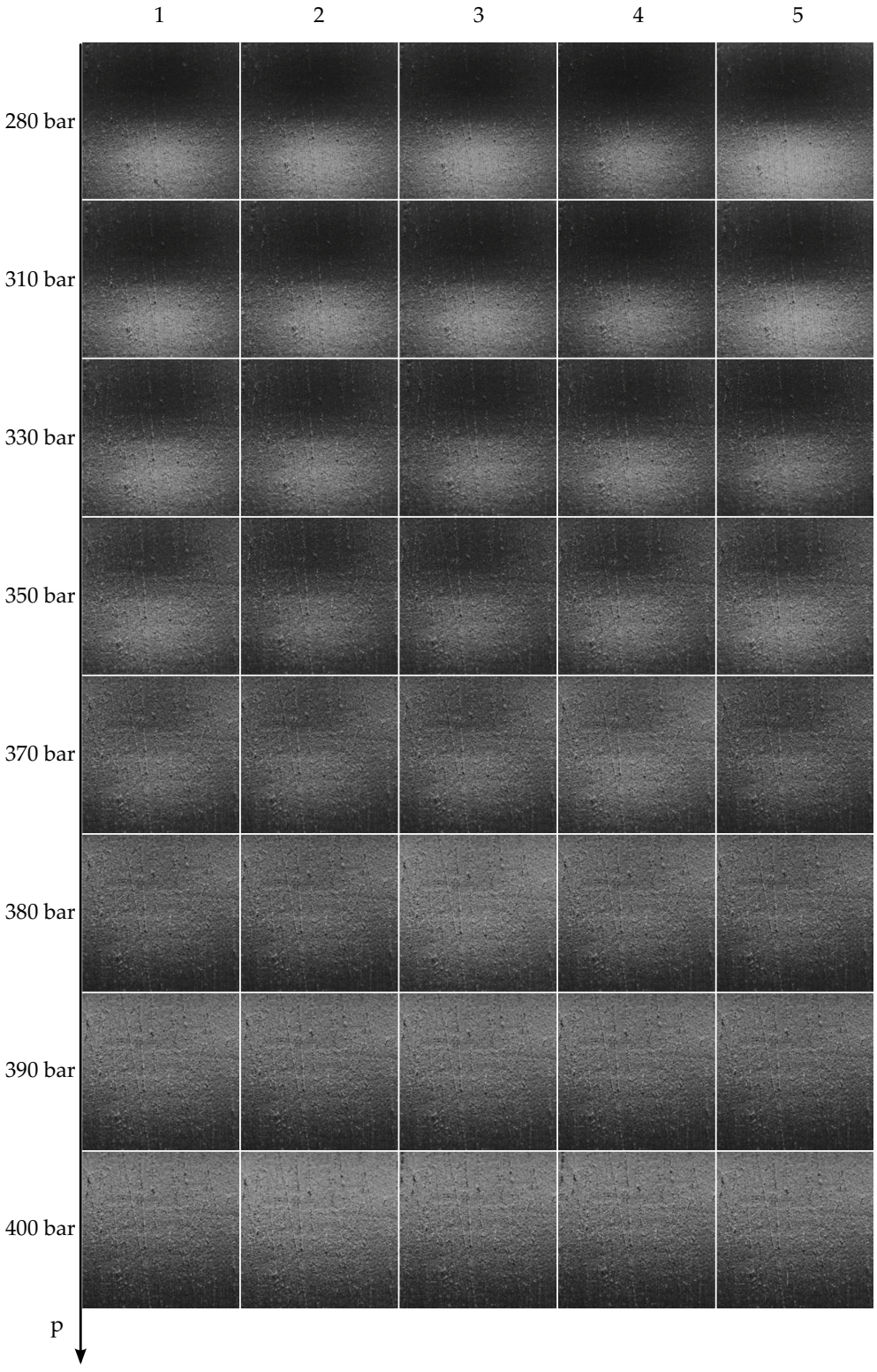

Figure 17: Array of captured images. Corresponding measurement results are displayed in Figure 18. The holding pressure increases from top to bottom. The rows display the images of the series of five specimens which were produced at the same respective holding pressure. The perceptibility threshold is found to be at a holding pressure of 390 bar in this example.

4.2 INFLUENCE OF THE INJECTION VELOCITY ON THE PERCEPTIBILITY OF SINK MARKS

It is common knowledge that high injection velocities increase the melt temperature depending on the induced shear strain, the material's viscosity and its thermal properties. Thereby, an influence on the formation of sink marks is to be expected. Similar to the test series mentioned in Section 4.1 a test series of specimens was produced where the injection velocity was increased from 50 cm^3/s to 130 cm^3/s in increments of 10 cm^3/s while the holding pressure was kept constant at 370 bar and the die temperature at 240 °C. The calibration of the test setup was the same as the one used for the measurements in Section 4.1. Figure 19 shows that, other than the variation of holding pressure, the variation of injection velocity exerts only low influence on the perceptibility of the sink marks.

As in Figure 18 the measuring points in Figure 19 each show the mean ASD value out of five measured specimens of the same production series. The variances were used as an estimate for the measurements' errors. As mentioned in Section 4.1, the calibration of the methodology was optimized for rather shallow sink marks. Since all sink marks in this test series produced ASDs below 1.5 x 10^{-4}, the errors of the results in Figure 19 are small.

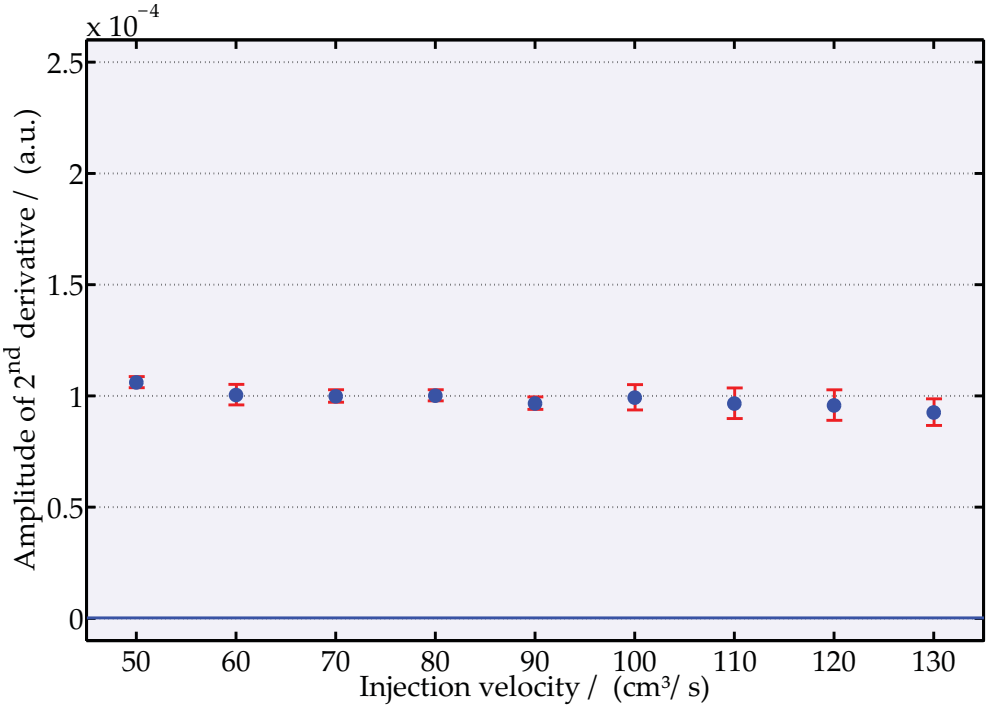

Figure 19: Measured ASD in dependence on injection velocity. The die temperature and the holding pressure were kept constant at 240 °C and 370 bar, respectively (cf. Figure 17). The measuring points each show the mean ASD value out of five measured specimens. The injection velocity was increased for each series from 50 cm^3/s to 130 cm^3/s in increments of 10 cm^3/s. The data shows that the injection velocity influences the perceptibility of the sink marks inconsiderably.

4.3 INTERRELATION OF THE HOLDING PRESSURE AND THE INJECTION VELOCITY

As mentioned in Section 4.1 and Section 4.2, the perceptibility of the sink marks is highly influenced by the holding pressure and almost inconsiderably by the injection velocity. In this section the interrelation of these two process parameters corresponding to the perceptibility of the sink mark is demonstrated.

As mentioned in Section 3.1.4, no parts were produced for holding pressures of 270 bar and 350 bar at injection velocities of 80 cm^3/s and 100 cm^3/s. Due to limited machine time and resources, all process parameter values could not be screened. The aforementioned process parameter values were assumed to be least important.

Figure 20 shows the measured ASDs over injection velocity for holding pressures of 230 bar to 390 bar. The influence of the holding pressure is much higher than the one of the injection velocity. Especially the decrease of perceptibility between 310 bar and 350 bar holding pressure is significant. Nevertheless, some influence of the injection velocity can be deduced from the measurements' data. Between 70 cm^3/s and 90 cm^3/s the perceptibility of the sink marks is constant while it increases for higher injection velocities at lower holding pressure levels. This increase is too little pronounced to draw conclusions from. Equivalent measurements at die temperatures of 230 °C and 240 °C and visual assessment show similar results.

In Figure 21 some images of the according sink marks are given in an array. For better clarity the sink marks formed at injection velocities of 80 cm^3/s and 100 cm^3/s are not displayed.

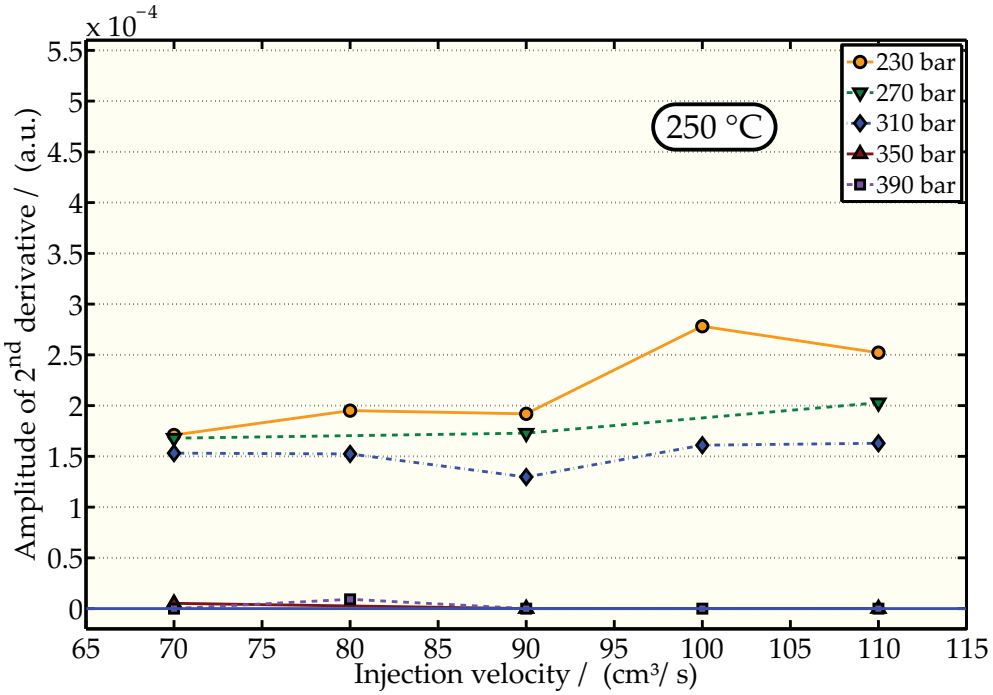

Figure 20: Measured ASD in dependence on injection velocity and holding pressure. The die temperature was kept constant at 250 °C for all measurements. The measuring points each show the mean ASD value out of five measured specimens.

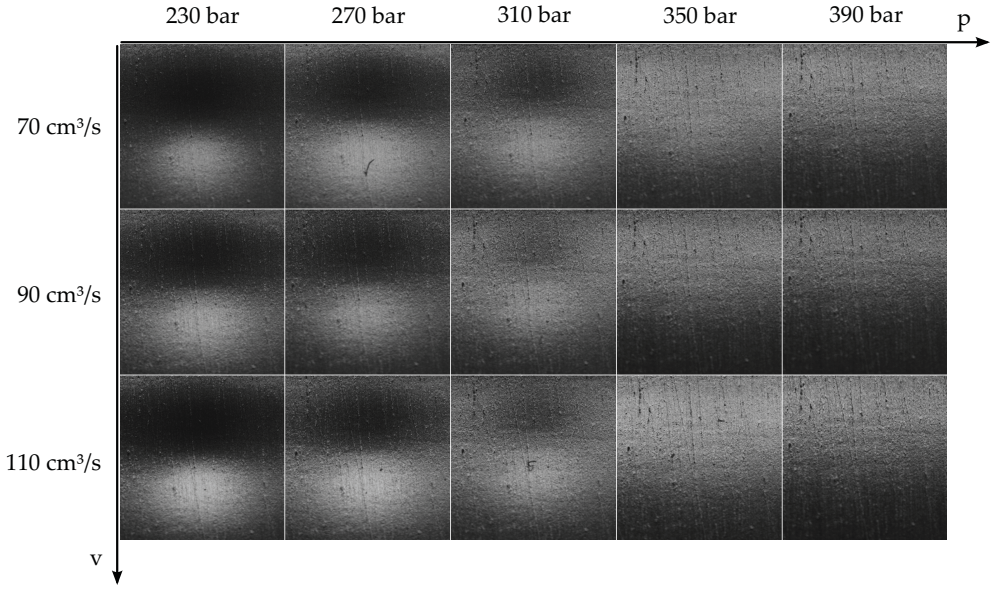

Figure 21: Array of sink marks according to the test results in Figure 20. The holding pressure increases from left to right, the injection velocity from top to bottom. The influence of the holding pressure exceeds the one of the injection velocity considerably.

4.4 INFLUENCE OF THE DIE TEMPERATURE ON THE PERCEPTIBILITY OF SINK MARKS

In this section the influence of the die temperature on the visibility of sink marks is shown. Die temperature is assumed to correspond to the melt temperature which could not be measured in a direct way. A lot of authors mention melt temperature as a "very influential parameter" but disagree if an increase of melt temperature reduces or produces the formation of sink marks. For example, Carley and Whittington, Ye and Leopold and Tursi and Bistany found that an increase in melt temperature produces sink marks[2] [34, 39, 43]. In contrast, Mathivanan and Parthasarathy found that an increase in melt temperature reduces sink marks[3] [18, 31, 38].

4.4.1 *Interrelation of the die temperature and the injection velocity*

In Figure 22 the influence of the die temperature in relation to the injection velocity is illustrated at a holding pressure of 230 bar. Die temperatures close to 240 °C, that is to say at the medium level, produced sink marks with highest perceptibility. It seems that this is due to two effects which oppose each other.
On the one hand more distinctive shrinking is advanced by higher melt temperature. Hence, it could be assumed that an increase in melt temperature leads to deeper sink marks.
On the other hand higher melt temperature causes comparatively elevated temperatures in the core of an injection molding part while its surface is cooled by the mold and freezes. Thus, the surface is more resistant to shrinking when the part's core freezes. Additionally, higher melt temperature causes longer effective holding pressure time as the gate freezes later and the viscosity of the melt is lower. Those assumptions could explain that an increase of melt temperature leads to shallower sink marks.
It may be that these effects combine worst at a certain temperature where sink marks are shallower both above and beyond it.

2 Carley and Whittington made this statement generally for all kinds of polymers. Ye and Leopold investigated sink marks using different kinds of polymers, where one of them was ABS. Tursi and Bistany used "both semi-crystalline and amorphous polymers".

3 Mathivanan and Parthasarathy simulated injection molding processes using the data of ABS polymers.

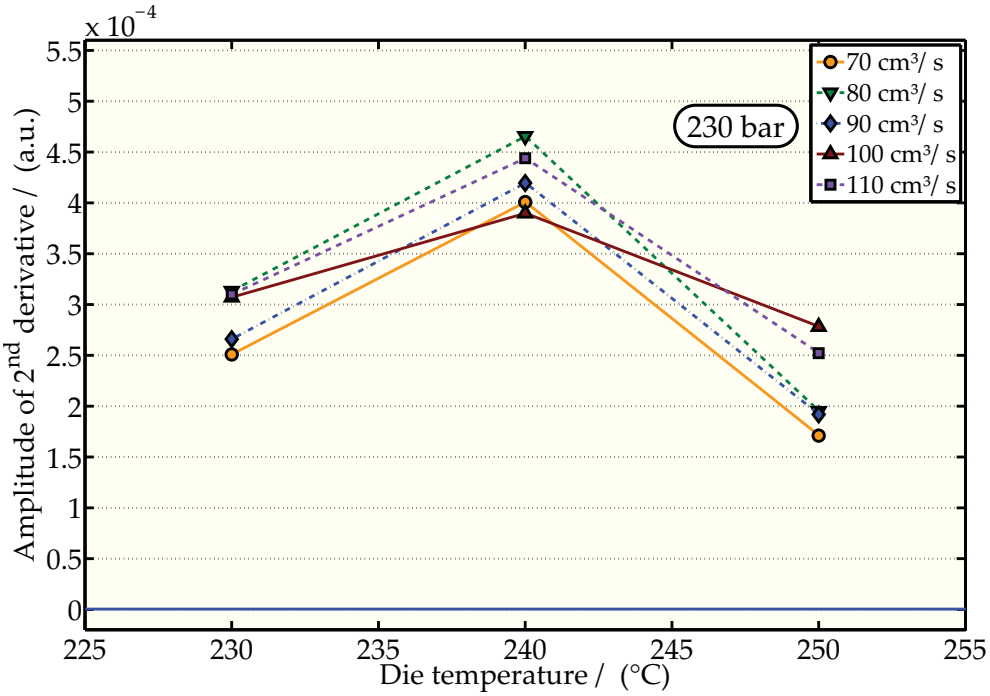

Figure 22: Measured ASD in dependence on die temperature for different levels of injection velocity. The holding pressure was kept constant at 230 bar. The measuring points each show the mean ASD value out of five measured specimens. The perceptibility was highest at a die temperature of 240 °C.

4.4.2 *Interrelation of the die temperature and the holding pressure*

Figure 23, Figure 24 and Figure 25 show the influence of the die temperature in dependence on the holding pressure for injection velocities of 70, 90 and 110 cm^3/s. The data in these figures shows similar behavior to the data in Figure 22 at holding pressures of 310 bar and below. The perceptibility of the sink marks decreases for higher holding pressures, in some cases below the perceptibility threshold. It seems that the mentioned effect of the longer holding pressure time due to higher die temperature (cf. Section 4.4.1) becomes more effective at higher holding pressures.

The measuring point at a holding pressure of 270 bar and a die temperature of 230 °C in Figure 23 is an unexpected measurement result as there is no familiar effect that would confirm this behavior. Visual assessment confirmed the strong visibility of this sink mark. Hence, it seems that this result is caused by irregularities in the production process (as mentioned in Section 3.1.4, there were process-related variations in the production process especially for these low die temperatures).

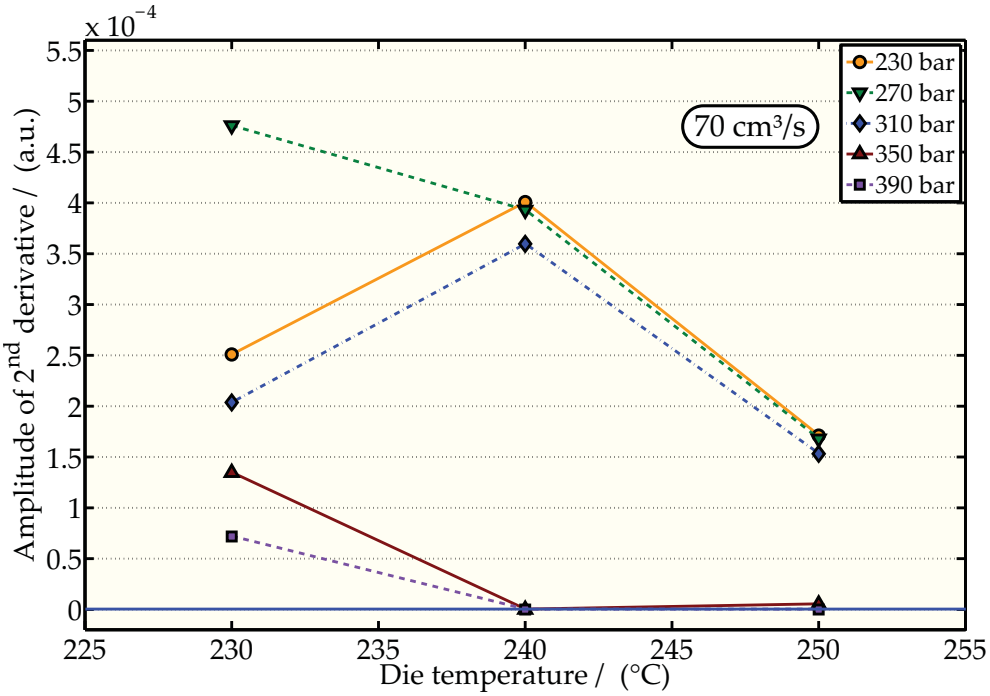

Figure 23: Measured ASD in dependence on die temperature. The injection velocity was kept constant at 70 cm^3/s. The measuring points each show the mean ASD value out of five measured specimens.

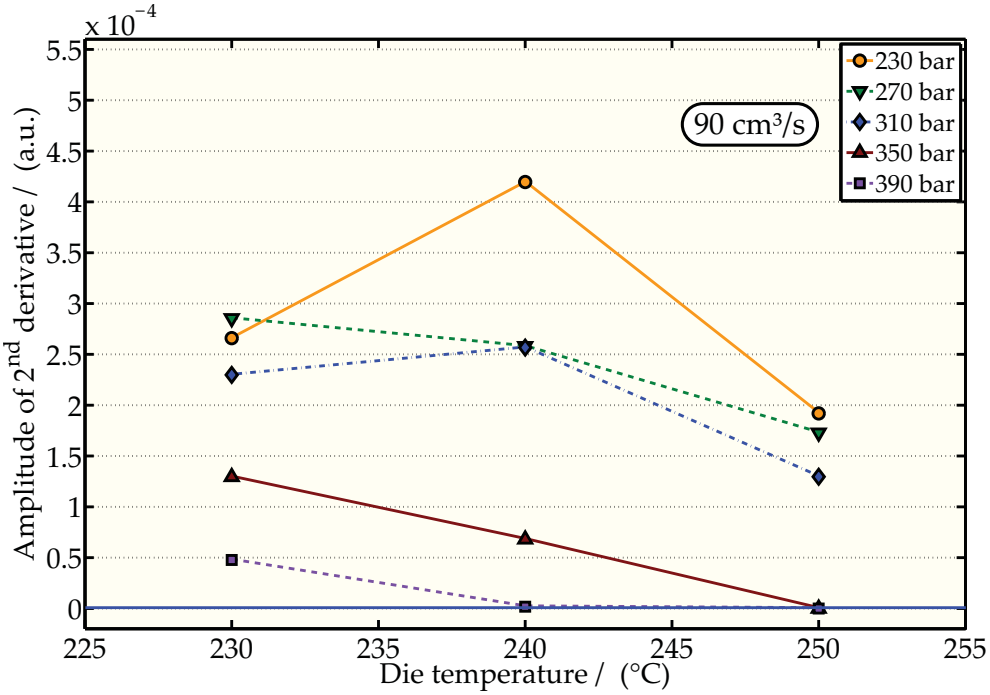

Figure 24: Measured ASD in dependence on die temperature. The injection velocity was kept constant at 90 cm^3/s. The measuring points each show the mean ASD value out of five measured specimens.

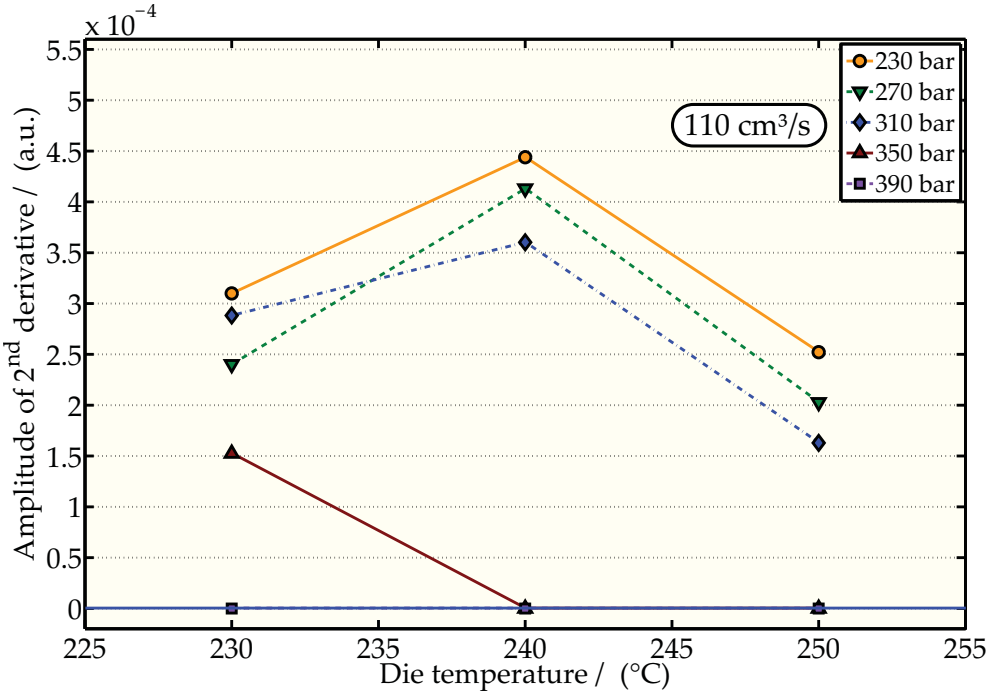

Figure 25: Measured ASD in dependence on die temperature. The injection velocity was kept constant at 110 cm^3/s. The measuring points each show the mean ASD value out of five measured specimens.

4.4.3 *Holding pressure series at varied die temperatures*

In Section 4.4.2 it was implied that higher die temperatures increase holding pressure time. This behavior causes low perceptibility of the sink marks at higher holding pressures. For better illustration, test series with varied holding pressure for die temperatures of 230 °C, 240 °C and 250 °C are displayed in Figure 26 and Figure 27. The injection velocity was kept constant at 90 cm^3/s and 110 cm^3/s, respectively.

The ASD decreases monotonically with increasing holding pressure in all measurements. Only at 230 °C deviations from this behavior can be seen for holding pressures between 230 bar and 310 bar. Since the calibration of the methodology was optimized for low sink mark perceptibility, it can be assumed that these deviations are caused for this reason.

As expected from the results in Section 4.4.2, the test series for the die temperature of 240 °C showed comparatively high perceptibility at low holding pressures. At high holding pressures the perceptibility decreases considerably. At 390 bar, for the injection velocity of 110 cm^3/s already at 350 bar, the perceptibility decreases below the perceptibility threshold.

At a die temperature of 230 °C the perceptibility decreases below the perceptibility threshold at 390 bar and 110 cm^3/s. At the injection velocity of 90 cm^3/s the perceptibility of the sink marks persists above the percepti-

bility threshold for all holding pressures. It seems that a higher injection velocity facilitates the influence of a higher holding pressure by increasing the melt temperature.

The test series at a temperature of 250 °C shows lower perceptibility than those at lower temperatures in each case. The perceptibility decreases below the perceptibility threshold at 350 bar for both injection velocities.

At an injection velocity of 110 cm^3/s all test series show a higher perceptibility than those at the injection velocity of 90 cm^3/s for lower holding pressure levels. The inverse behavior is observed at higher holding pressure levels. As mentioned in Section 4.4.2, a higher temperature prolongs holding pressure time. At high holding pressure this becomes the predominant factor leading to considerably low perceptibility of the sink marks.

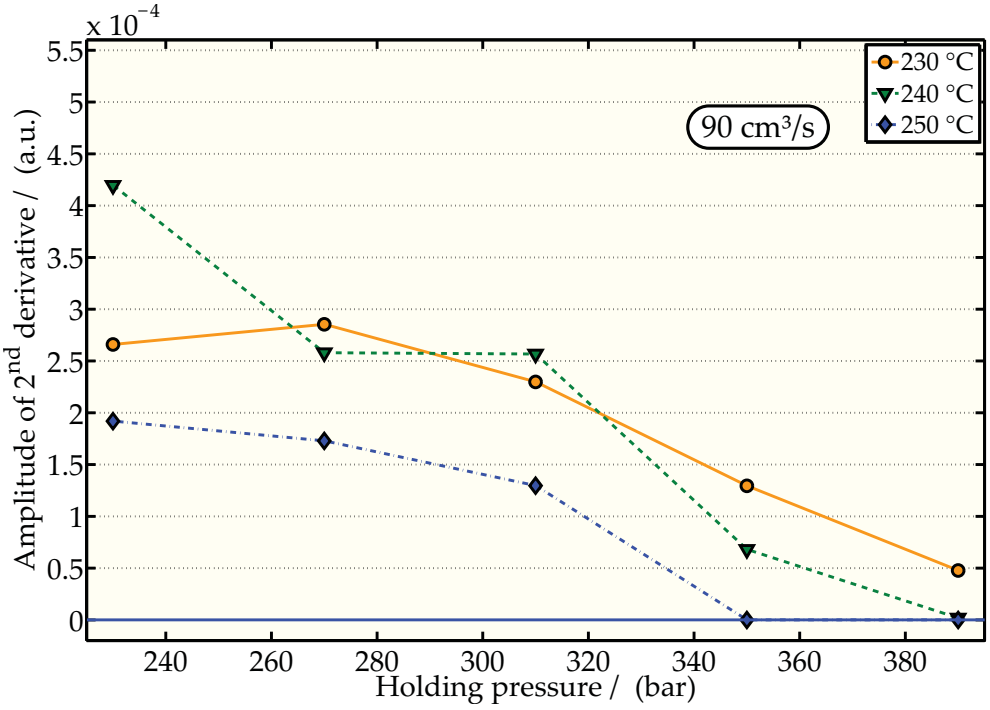

Figure 26: Measured ASD in dependence on holding pressure for die temperatures of 230 °C to 250 °C. The injection velocity was kept constant at 90 cm^3/s for all measurements. The measuring points each show the mean ASD value out of five measured specimens.

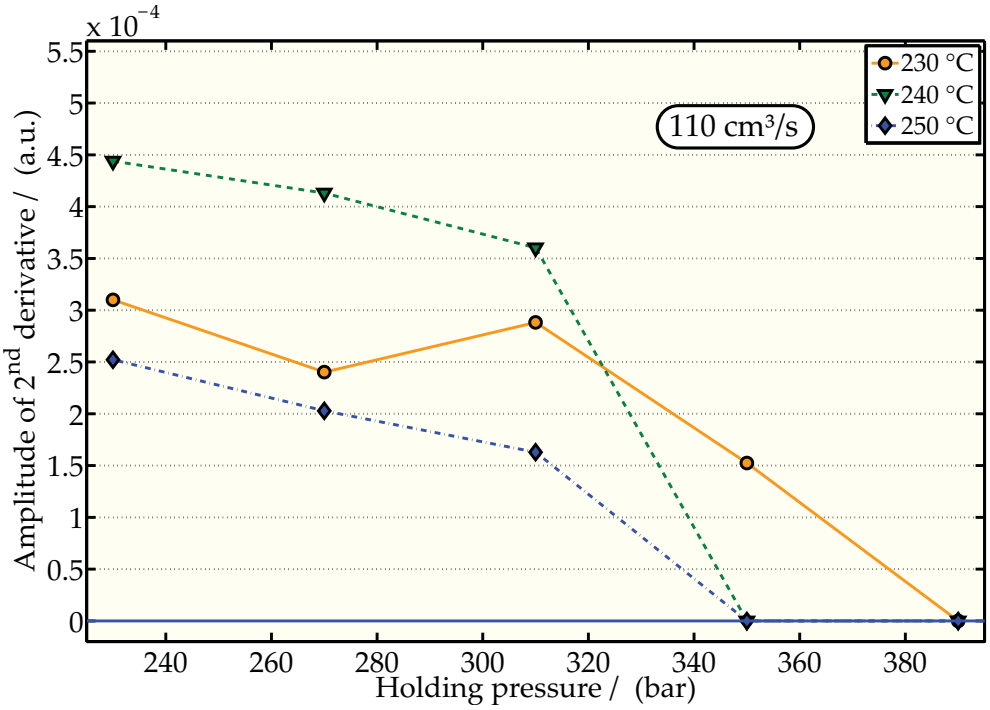

Figure 27: Measured ASD in dependence on holding pressure for die temperatures of 230 °C to 250 °C. The injection velocity was kept constant at 110 cm^3/s for all measurements. The measuring points each show the mean ASD value out of five measured specimens.

4.5 INFLUENCE OF THE COOLANT TEMPERATURE ON THE PERCEPTIBILITY OF SINK MARKS

In this section the influence of the coolant temperature on the perceptibility of the sink marks is examined. Higher temperatures of the mold result in slower and more uniform cooling. Thereby, the surfaces of injection molded parts are comparatively less resistant to deformation when the sealing point is reached. So it is expected that higher mold temperature facilitates the formation of sink marks. Additionally, the shrinking increases with higher temperatures. This view is also supported by literature [18, 31, 34, 38, 43].

As mentioned in Section 3.1.4, the mold temperature exhibits strong variations during an injection molding cycle and is not independent of the other injection molding parameters. Therefore, the coolant temperature was used instead as a parameter for the given test series which allows to draw conclusions about the influence of the mold temperature from it. The die temperature was kept constant at 240 °C for all measurements.

Figure 28 and Figure 29 present the perceptibility of the sink marks in dependence on injection velocity for holding pressures of 230 bar to 390 bar at coolant temperatures of 40 °C and 50 °C, respectively. The die temperature was kept constant at 240 °C.

There is a minor influence of the injection velocity on the perceptibility of the sink marks, while the holding pressure's influence is strong. For this reason, it is not possible to deduce an unambiguous dependence of the perceptibility as a function of injection velocity for both coolant temperatures.

At a coolant temperature of 40 °C the perceptibility decreases below the perceptibility threshold at injection velocities of 70 cm^3/s and 110 cm^3/s and at a holding pressure of 350 bar and higher. At an injection velocity of 90 cm^3/s the perceptibility is higher than the perceptibility threshold for a holding pressure of 350 bar. No substantial reason could be found for this unexpected behavior.

The perceptibility increases considerably for the same values of injection velocity and holding pressure at a coolant temperature of 50 °C. As mentioned before, the higher mold temperature reduces the temperature differences between the surface and the core of the part. This leads to decreased stiffness of the surface at sealing point. Thereby, sink marks seem to be formed more easily.

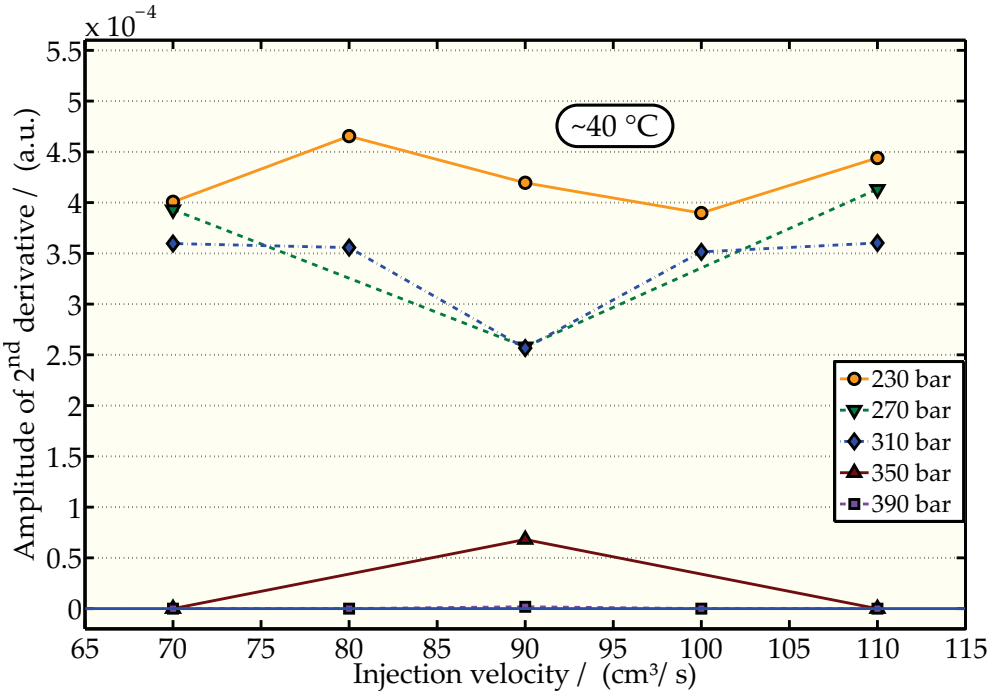

Figure 28: Measured ASD in dependence on injection velocity for holding pressures of 230 bar to 390 bar. The coolant temperature was kept constant at 40 °C for all measurements. The die temperature was kept constant at 240 °C. The measuring points each show the mean ASD value out of five measured specimens.

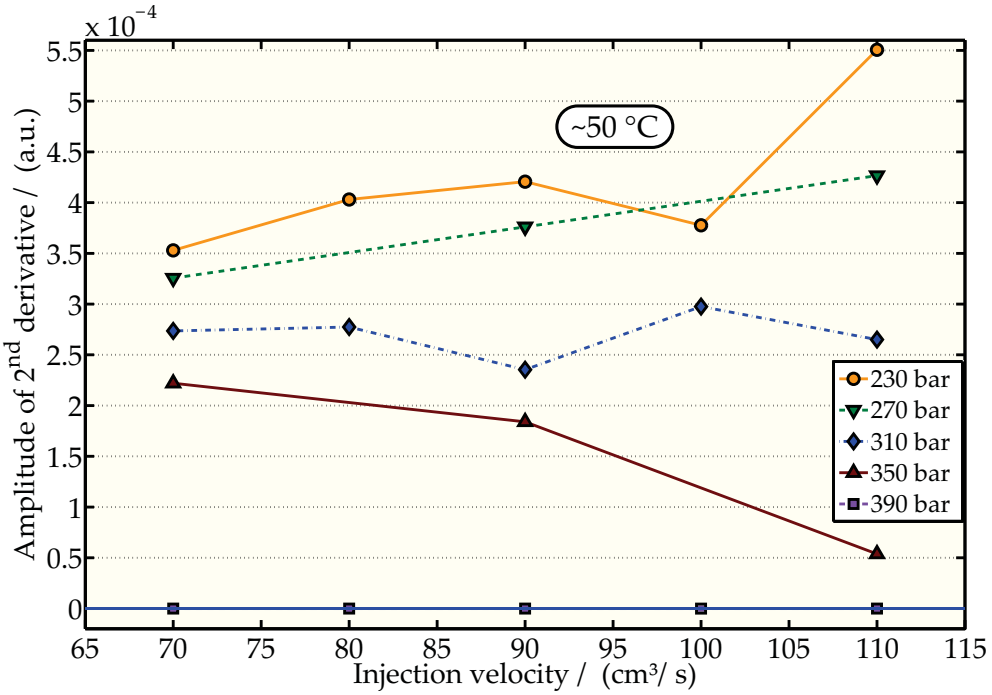

Figure 29: Measured ASD in dependence on injection velocity for holding pressures of 230 bar to 390 bar. The coolant temperature was kept constant at 40 °C for all measurements. The die temperature was kept constant at 240 °C. The measuring points each show the mean ASD value out of five measured specimens.

Figure 30, Figure 31 and Figure 32 display the perceptibility in dependence on the holding pressure for coolant temperatures of 40 °C and 50 °C at injection velocities of 70 cm^3/s, 90 cm^3/s and 110 cm^3/s, respectively. The die temperature was kept constant at 240 °C. At injection velocities of 70 cm^3/s and 110 cm^3/s the perceptibility shows linear behavior for lower holding pressures and decreases below the perceptibility threshold at holding pressures of 350 bar and 390 bar for coolant temperatures of 40 °C and 50 °C, respectively. The perceptibility decreases below the perceptibility threshold at an injection velocity of 90 cm^3/s and a holding pressure of 390 bar for coolant temperatures of 40 °C and 50 °C each.

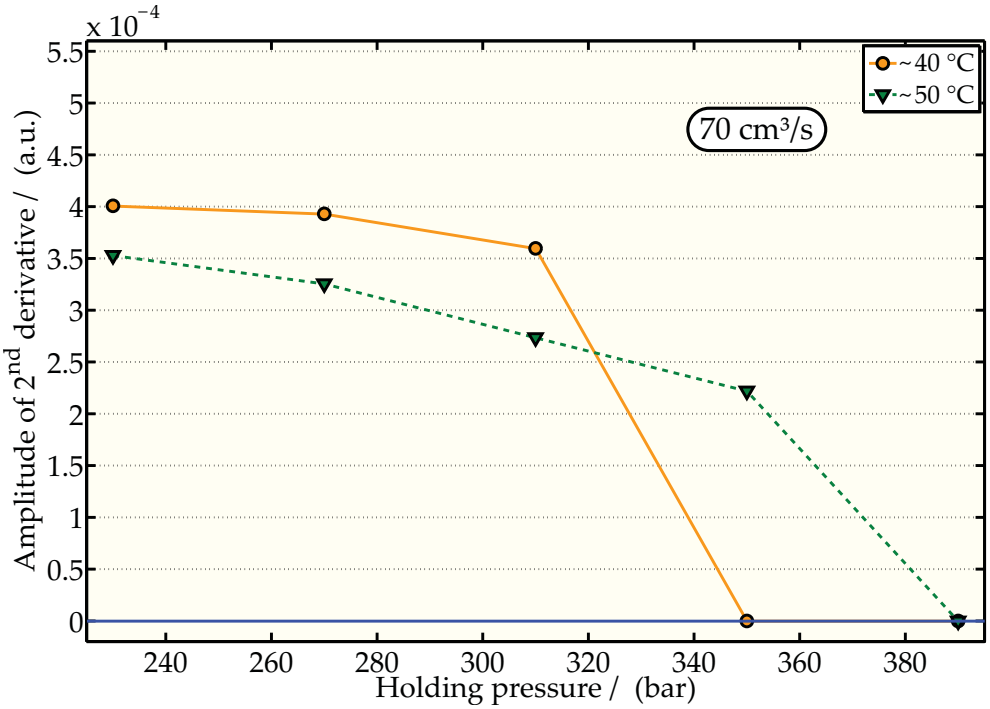

Figure 30: Measured ASD in dependence on holding pressure for coolant temperatures of 40 °C and 50 °C. The injection velocity was kept constant at 70 cm^3/s for all measurements. The die temperature was kept constant at 240 °C. The measuring points each show the mean ASD value out of five measured specimens.

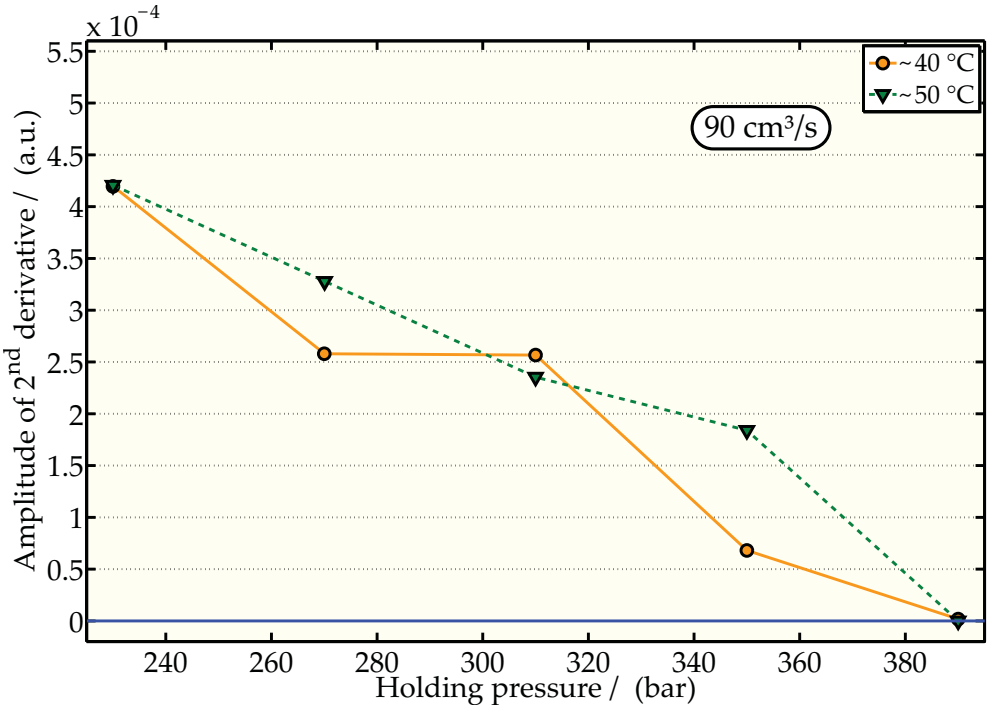

Figure 31: Measured ASD in dependence on holding pressure for coolant temperatures of 40 °C and 50 °C. The injection velocity was kept at 90 cm^3/s and the die temperature at 240 °C. The ASD is the mean ASD value out of five specimens.

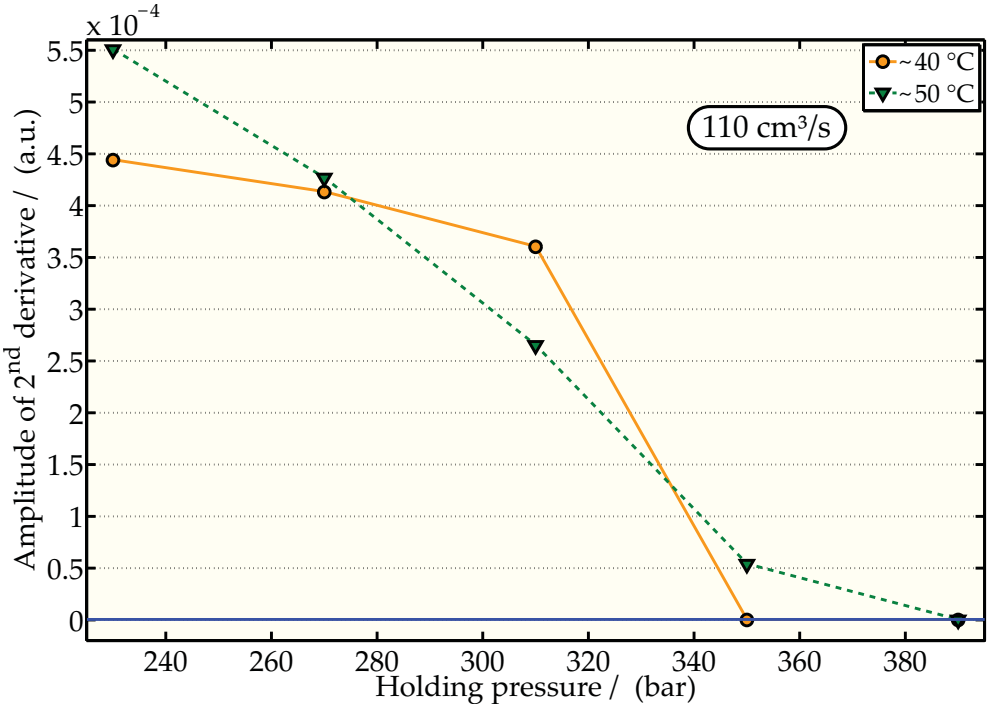

Figure 32: Measured ASD in dependence on holding pressure for coolant temperatures of 40 °C and 50 °C. The injection velocity was kept at 110 cm^3/s and the die temperature at 240 °C. The ASD is the mean ASD value out of five specimens.

4.6 ROBUSTNESS OF THE MEASUREMENT RESULTS

In order to prove the robustness of the surface inspection methodology, test series were performed. For this purpose, single samples were selected and each measured several times. Then each series was evaluated separately. This approach was chosen to separate influences of the molding process from the measurement errors of the methodology. This allowed direct evaluation of the sink mark inspection inaccuracies of the methodology including impreciseness of specimen positioning. The errors caused by imprecise positioning can be reduced considerably by using a robot system for the part handling.

Four parts with different perceptibility of the sink marks were selected for the test series. The parts were produced at holding pressures of 320 bar, 360 bar, 380 bar, and 390 bar, where the injection velocity was kept constant at 90 cm^3/s, the die temperature at 240 °C and the coolant temperature at 40 °C. Each part was measured 30 times in series while it was removed and positioned again for each measurement.

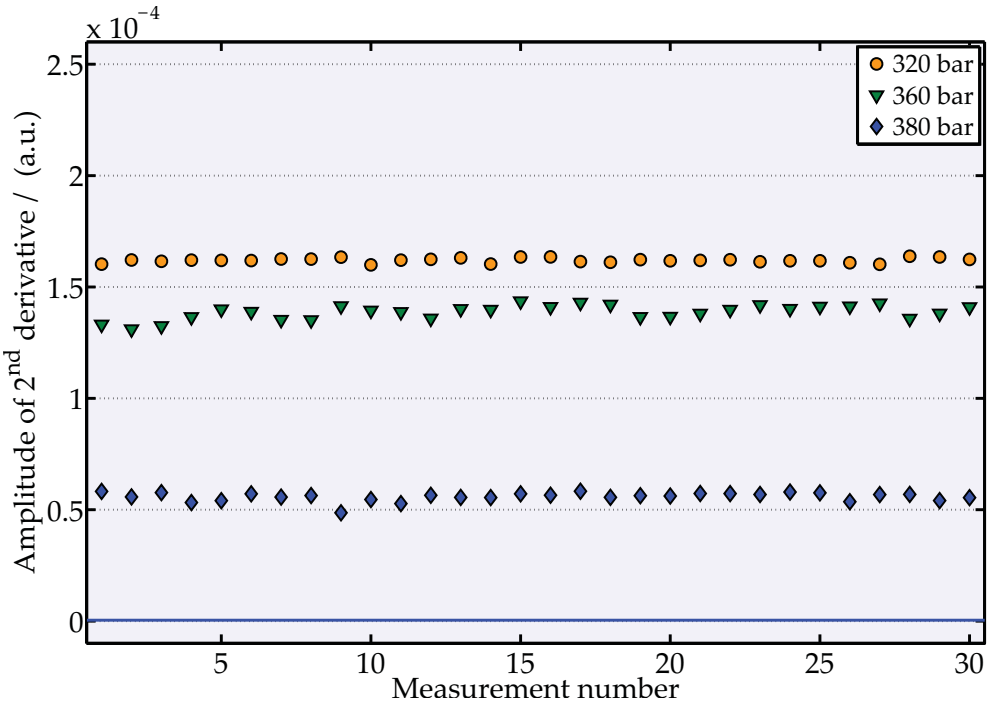

Figure 33: Robustness analysis of the used methodology. Four different sink marks were measured 30 times each to check the robustness of the measurement system. The relative errors amount to 0.6 % (320 bar), 2.3 % (360 bar) and 3.6 % (380 bar). For a holding pressure of 390 bar, there was no sink mark detected in each of the 30 measurements.

As displayed in Figure 33 the measured series show fairly consistent results. The relative errors are 0.6 % (320 bar), 2.3 % (360 bar), and 3.6 % (380 bar). For a holding pressure of 390 bar, there was no sink mark detected in each of the 30 measurements[4]. It has to be concluded that such good results are only achievable by extremely accurate calibration of the inspection system.

4 Of course, an estimation of the relative errors was not possible for a holding pressure of 390 bar, since there was no sink mark detected in each of the measurements.

5 CONCLUSION

The objective of this work was to contribute to the improvement of a methodology for the evaluation of the visual perceptibility of sink marks on injection molded parts by a machine vision system. For this purpose, parts consisting of ABS Terluran 958I® were produced using several varied process parameters. Based on a concept developed by Gruber, an alternative methodology to acquire images of sink marks was developed [19]. The intensity matrix of these images was approximated by a surface function. Using this surface function, a model parameter was used to evaluate the visibility of the sink marks.

The methodology shows good performance while keeping measurement errors small. It is robust concerning the influence of ambient light and surface damages like scratches. The process time is small enough to allow an application in injection molding processes.
However, the measurement setup that was constructed during this work is sensitive to imprecise calibration. In an industrial application, this problem should be manageable due to automation.

Influences of holding pressure, injection velocity, die temperature and coolant temperature on the formation of sink marks were studied using this methodology. The results show that injection velocity influences the formation of sink marks inconsiderably. Because of the strong influence of other parameters like holding pressure or die temperature on the perceptibility of the sink marks no unambiguous conclusion can be drawn on the influence of injection velocity. Because of heating of the melt due to high injection velocities its influence on the perceptibility seems to be similar to the influence of small variations in the die temperature.

It seems that two effects which influence the perceptibility in opposite directions are related to die temperature. On the one hand more distinctive shrinking is facilitated by a high melt temperature. On the other hand high melt temperature causes elevated temperatures in the center of an injection molding part when its surface freezes. While the surface is already resistant to shrinking to a large extent, the higher temperatures of the die and the center of the parts prolong holding pressure time by ensuring that the gate freezing is retarded. Hence, there seem to be two different effects that combine worst at a certain temperature. As mentioned, Mathivanan and Parthasarathy found in several papers that high mass temperature decreases the formation of sink marks, which is a contradiction to the findings of Carley and Whittington and other authors who each found that high mass temperature increases sink mark formation [18, 31, 34, 38, 39, 43]. Results of

the given work show that increasing the melt temperature can both increase and decrease the visibility of sink marks. Further research work is necessary to confirm this assumption.

Higher temperature of the mold results in slower and more uniform cooling. Thereby, the surfaces of injection molded parts seem to be comparatively less resistant to deformation when the sealing point is reached. So it is expected that higher coolant temperatures advance the formation of sink marks. This behavior could be deduced from the results in this work.

In this work, holding pressure was found to be the major influence on the perceptibility of the sink marks within the given process latitude and for the given injection molded part.

It was shown that holding pressure strongly influences the visibility of sink marks as higher holding pressure reduces the formation of sink marks clearly. As can be seen, it has the biggest influence among the investigated parameters.

Furthermore, it was shown that the influence of injection velocity on formation of sink marks is minor.

It is suggested to increase holding pressure to avoid the formation of sink marks. The influence of the melt temperature on the formation of sink marks is high. However, it is not possible to make a clear statement about if it should be increased or decreased to reduce sink marks. Variation of injection velocity or mold temperature does not seem to be a useful method to avoid sink marks within the investigated process window.

As a next step, it is recommended to examine whether an increase in melt temperature produces or reduces sink marks. Therefor, the depth of produced sink marks should be measured as exact as possible, for example using confocal microscopy. Further, to improve the inspection system, one should find a way to avoid the high sensitivity to imprecise positioning.

LIST OF FIGURES

LIST OF TABLES

ACRONYMS

ABS acrylonitrile butadiene styrene

ASD amplitude of the second derivative

ASA acrylester styrene acrylonitrile

CCD charge-coupled device

PCCL Polymer Competence Center Leoben GmbH

BIBLIOGRAPHY

[1] K. Ishii, K. Beiter, and L. Hornberger. Sink marks in crossed ribs. *Technical Papers*, 50:2434–2436, 1992. (Cited on page 1.)

[2] Linhuo Shi and Mahesh Gupta. Prediction of sink mark in injection-molded plastic parts using a localized shrinkage model near a rib. In *ANTEC 1998*, pages 609–613, Houghton, Michigan, 1998. Mechanical Engineering and Engineering Mechanics Department Michigan Technological University, Society of Plastics Engineers. (Cited on page 2.)

[3] Linhuo Shi and Mahesh Gupta. A localized shrinkage analysis for predicting sink marks in injection-molded plastic parts. *The Journal of Injection Molding Technology*, 2(4):149–155, December 1998. URL http://www.4plasticsresearch.com/abstract.php?id=ij129800149.pdf&type=hitlist&num=1. last viewed on 2010-07-09.

[4] Linhuo Shi and Mahesh Gupta. An approximate prediction of sink mark depth in rib-reinforced plastic parts by empirical equations. *The Journal of Injection Molding Technology*, 3(1):1–10, 1999. URL http://cat.inist.fr/?aModele=afficheN&cpsidt=2004017. last viewed on 2010-07-09.

[5] Linhuo Shi and Mahesh Gupta. Prediction of sink marks in cross-rib-reinforced injection-molded plastic parts by localized finite element shrinkage analysis. *The Journal of Injection Molding Technology*, 3(3): 108–116, September 1999. URL http://www.4plasticsresearch.com/abstract.php?id=ij099900108.pdf&type=hitlist&num=0. last viewed on 2010-07-09.

[6] Linhuo Shi and Mahesh Gupta. Empirical equations for predicting sink mark depth in a rib-reinforced plastic part. In *ANTEC 1999*, pages 815–819, Houghton, Michigan, 1999. Mechanical Engineering and Engineering Mechanics Department Michigan Technological University, Society of Plastics Engineers. URL http://www.4plasticsresearch.com/abstract.php?id=1999-0592.pdf&type=hitlist&num=5. last viewed on 2010-07-09.

[7] Linhuo Shi and Mahesh Gupta. Modeling of sink mark formation in cross-rib-reinforced injection-molded plastic parts by localized finite element shrinkage analysis. In *ANTEC 2000*, Houghton, Michigan, 712–715 2000. Mechanical Engineering and Engineering Mechanics Department Michigan Technological University, Society of Plastics Engineers. URL http://www.4plasticsresearch.com/abstract.php?id=2000-0739.pdf&type=hitlist&num=4. last viewed on 2010-07-09. (Cited on pages 1 and 2.)

[8] J.C. Moller and J.J. Rowe. Prediction of injection molded part quality by neural networks. In *ANTEC 1998*. Society of Plastics Engineers, 1998. (Cited on page 2.)

[9] Faezeh Soltani and Souran Manoochehri. Prediction of the weld lines in injection molding process using neural networks. In *ANTEC 2000*, Hoboken, New Jersey, 2000. Society of Plastics Engineers. URL http://www.4plasticsresearch.com/abstract.php?id=2000-0372.pdf&type=hitlist&num=0. last viewed on 2010-07-22. (Cited on page 2.)

[10] Shijun Ni. Preventing sink marks of injection molded parts using CAE analysis. In *ANTEC 2000*, pages 453–455, Lexington, Kentucky, 2000. Lexmark International Inc., Society of Plastics Engineers. URL http://www.4plasticsresearch.com/abstract.php?id=2000-0271.pdf&type=hitlist&num=11. last viewed on 2010-07-09. (Cited on page 2.)

[11] Stéphane Mérillou, Jean-Michel Dischler, and Djamchid Ghazanfarpour. Surface scratches: measuring, modeling and rendering. *The Visual Computer*, 17(1):30–45, February 2001. URL http://www.springerlink.com/content/8nnvv1t2xqcqp15d/. last viewed on 2010-07-23. (Cited on page 2.)

[12] Franz Pernkopf and Paul O'Leary. Visual inspection of machined metallic high-precision surfaces. *Journal on Applied Signal Processing*, 7:667–678, January 2002. (Cited on page 2.)

[13] Raimo Silvennoinen, Kari Myller, Kai-Erik Peiponen, Jaakko Salmi, and Esko J. Pääkkönen. Diffractive optical sensor for gloss differences of injection molded plastic products. *Sensors and Actuators A*, 112:74–79, 2004. (Cited on page 2.)

[14] Kurt Frederic Hayden and Paul V. Engelmann. Smoke and mirrors: hiding sink in plain sight. In *ANTEC 2008*, pages 703–707, Houston and Kalamazoo, 2008. Society of Plastics Engineers. URL http://plasticsengineering.org/node/1548. last viewed on 2010-07-08. (Cited on pages 2, 19, and 20.)

[15] Kurt Frederic Hayden. *Determining the probability of the visual detection of sink marks on differently textured injection molded products*. Dissertation, Western Michigan University, Kalamazoo, Michigan, December 2006. (Cited on pages 2 and 20.)

[16] Hongsheng Li, Zhiying Guo, and Dequn Li. Reducing the effects of weldlines on appearance of plastic products by Taguchi experimental method. *The International Journal of Advanced Manufacturing Technology*, 32:927–931, 2007. doi: 10.1007/s00170-006-0411-z. URL http://www.springerlink.com/content/51625l6654v3433t/. last viewed on 2010-07-08. (Cited on page 2.)

[17] Xianghua Xie. A review of recent advances in surface defect detection using texture analysis techniques. *Electronic Letters on Computer Vision and Image Analysis*, 7(3):1–22, April 2008. URL http://elcvia.cvc.uab.cat/index.php/elcvia/article/viewFile/268/176. last viewed on 2010-07-21. (Cited on page 3.)

[18] D. Mathivanan and N.S. Parthasarathy. Prediction of sink depths using nonlinear modeling of injection molding variables. *The International Journal of Advanced Manufacturing Technology*, 43(7):654–663, August 2009. doi: 10.1007/s00170-008-1749-1. URL http://dx.doi.org/10.1007/s00170-008-1749-1. last viewed on 2010-07-08. (Cited on pages 3, 20, 21, 41, 48, 54, and 60.)

[19] Dieter P. Gruber. Verfahren zum automatischen Nachweis eines Defektes an der Oberfläche eines Formteils, 2009. A384. (Cited on pages 3, 37, 38, and 60.)

[20] Gernot Pacher. On the evaluation of the visual impact of sink marks of injection molded parts. Master's thesis, Montanuniversität Leoben, Leoben, Austria, August 2009. (Cited on pages 3, 28, 37, 38, and 39.)

[21] Dieter P. Gruber, Gernot Wallner, and Michael Buder-Stroissnig. Verfahren zur Analyse der Oberflächeneigenschaften eines Materials, June 2005. A1036.

[22] Dieter P. Gruber, Gerald Berger, Gernot Pacher, and Walter Friesenbichler. Novel approach to the measurement of the visual perceptibility of sink marks on injection molding parts. 2011. (Cited on page 3.)

[23] Rafeal C. Gonzales and Richard E. Woods. *Digital Image Processing*. Robbins, Tom, New Jersey, second edition, January 2002. (Cited on pages 5, 7, 8, and 9.)

[24] Bernd Jähne. *Digital Image Processing*. Springer-Verlag, Heidelberg, Germany, fifth revised and extended edition, April 2002. (Cited on pages 6 and 7.)

[25] William K. Pratt. *Digital Image Processing. PIKS Scientific inside*. Wiley-Interscience, Los Altos, California, fourth edition, 2007. (Cited on page 8.)

[26] Jaan Kiusalaas. *Numerical Methods in Engineering with MATLAB®*. Cambridge University Press, The Pennsylvania State University, 2005. URL http://www.cambridge.org/gb/knowledge/isbn/item1172922/?site_locale=en_GB. last viewed on 2010-01-17. (Cited on page 11.)

[27] Stefan Adam. *MATLAB® und Mathematik kompetent einsetzen. Eine Einführung für Ingenieure und Naturwissenschaftler*. Wiley-VCH, Zürich, Switzerland, 2006. (Cited on page 11.)

[28] Siegfried Stitz and Walter Keller. *Spritzgießtechnik: Verarbeitung, Maschinen, Peripherie*. Hanser Verlag, Germany, second edition, 2004. (Cited on page 13.)

[29] Martin Vines and Prithu Mukhopdhyay. Plastic facts – numbers that count. Published in PlasticTrends.net, July 2010. URL http://www.plasticstrends.net/index.php?option=com_content&view=article&id=39:numbers-that-count&catid=7:plastics-facts&Itemid=33. last viewed on 2010-07-08. (Cited on page 13.)

[30] Technisches Datenblatt ENGEL ES 330/80 H. *Technische Daten*. ENGEL Austria GmbH, Schwertberg, Austria, 1992. (Cited on page 13.)

[31] D. Mathivanan and N.S. Parthasarathy. Sink mark prediction and optimization – a review. In *ANTEC 2008*, pages 2126–2132, Chennai, India, 2008. Society of Plastics Engineers. URL http://plasticsengineering.org/sites/default/files/0243.pdf. last viewed on 2010-07-08. (Cited on pages 14, 19, 20, 21, 41, 48, 54, and 60.)

[32] *Specification of Terluran 958I®*. IDES – The Plastics Web®, January 2009. (Cited on pages 15 and 65.)

[33] *Specification of Terluran 958I®*. MatWeb – Material Property Data®, March 2010. (Cited on pages 15 and 65.)

[34] James F. Carley and Lloyd R. Whittington. *Whittington's dictionary of plastics*. Technomic Publishing Company, Inc., Lancester, Pennsylvania, third edition, 1993. (Cited on pages 19, 20, 41, 48, 54, and 60.)

[35] VDI-Gesellschaft Kunststofftechnik. *Injection moulding technology*. Verein Deutscher Ingenieure, Düsseldorf, Germany, 1981. (Cited on page 19.)

[36] Donald V. Rosato and Dominick V. Rosato. *Injection molding handbook*. Chapman & Hall, New York, second edition, 1995. (Cited on page 19.)

[37] K. Nakayama, M. Kodama, and Motoichi. Optimization of rib design and possibilities of weight reduction for ABS moldings. *Technical Papers*, 41:690–693, 1983. (Cited on page 20.)

[38] D. Mathivanan and N.S. Parthasarathy. Sink-mark minimization in injection molding through response surface regression modeling and genetic algorithm. *The International Journal of Advanced Manufacturing Technology*, 45(9):867–874, December 2009. doi: 10.1007/s00170-009-2021-z. URL http://www.springerlink.com/content/pl774x7n0425r440. last viewed on 2010-07-08. (Cited on pages 20, 41, 48, 54, and 60.)

[39] H. Ye and P.M. Leopold. Minimizing part sink marks using c-mold and genetic optimization algorithm. *Technical Papers*, 58:589–593, 2000. (Cited on pages 20, 48, and 60.)

[40] Robert A. Malloy. *Plastic part design for injection molding: an introduction*. Hanser Verlag, Lowell, Massachusetts, 1994. (Cited on page 20.)

[41] M.J. Liou, D.M. Ramachandra, K. Ishii, and L. Hornberger. Sink mark study in injection molded parts. In *ANTEC 90*, pages 288–291, Dallas, Texas, May 1990. Society of Plastics Engineers. URL http://md1.csa.com/partners/viewrecord.php?requester=gs&collection=TRD&recid=9104E1P0210EP. last viewed on 2010-07-22. (Cited on page 21.)

[42] Changyu Shen, Lixia Wang, Wei Cao, and Li Qian. Investigation of the effect of molding variables on sink marks of plastic injection molded parts using Taguchi DOE technique. *Polymer-Plastics Technology and Engineering*, 46(3):219–225, March 2007. (Cited on page 21.)

[43] Dan Tursi and S.P. Bistany. Process and tooling factors affecting sink marks for amorphous and crystalline resins. *The Journal of Injection Molding Technology*, 4(3):114–119, September 2000. URL http://md1.csa.com/partners/viewrecord.php?requester=gs&collection=TRD&recid=200106E1P0184EP. last viewed on 2010-07-08. (Cited on pages 21, 48, 54, and 60.)

[44] Lixia Wang, Qian Li, Changyu Shen, and Shufen Lu. Effects of process parameters and two-way interactions on sink mark depth of injection molded parts by using the design of experiment method. *Polymer-Plastics Technology and Engineering*, 47(1):30–35, January 2008. URL http://www.informaworld.com/smpp/content~db=all~content=a789005986. last viewed on 2010-07-22. (Cited on pages 21 and 41.)

[45] *Specification of PENTAX C2514-M(KP), 25 mm, 1:1.4*. PENTAX Precision Co.,Ltd., 2003. URL http://www.theimagingsource.com/downloads/c2514mkp.en_US.pdf. last viewed on 2010-07-08. (Cited on page 22.)

[46] Directed area lights. *vicolux® FAL11 series 240 × 180 mm² shining area*. Vision & Control GmbH, Suhl, Germany, Version 2.0.2. URL http://www.vision-projekt.de/Bildverarbeitung/Produkte.nsf/0/F221093F0BB831D7C1257671002AB57B?Open&Lang=DEtop. last viewed on 2010-07-08. (Cited on page 22.)

[47] L.R. Ingersoll. A means to measure the glare of paper. *Electr. World*, 63: 645–647, 1914. (Cited on page 22.)

[48] MATLAB® product help. *function demosaic*. The MathWorks Inc., R2009b. URL http://www.mathworks.com/access/helpdesk/help/toolbox/images/demosaic.html. last viewed on 2010-07-08. (Cited on page 23.)

[49] MATLAB® product help. *function rgb2gray*. The MathWorks Inc., R2009b. URL http://www.mathworks.com/access/helpdesk/help/

toolbox/images/imregionalmax.html. last viewed on 2010-07-08. (Cited on page 26.)

[50] Dietmar Haba, Dieter P. Gruber, and Johannes Macher. Defect visibility measurement program. PCCL, 2010. (Cited on page 27.)

[51] MATLAB® product help. *function fit*. The MathWorks Inc., R2009b. URL http://www.mathworks.com/access/helpdesk/help/toolbox/curvefit/fit.html. last viewed on 2010-07-08. (Cited on page 28.)

[52] MATLAB® product help. *function imregionalmax*. The MathWorks Inc., R2009b. URL http://www.mathworks.com/access/helpdesk/help/toolbox/images/imregionalmax.html. last viewed on 2010-07-08. (Cited on pages 28 and 38.)

[53] MATLAB® product help. *function imregionalmin*. The MathWorks Inc., R2009b. URL http://www.mathworks.com/access/helpdesk/help/toolbox/images/imregionalmin.html. last viewed on 2010-07-08. (Cited on pages 28 and 38.)

[54] Gerald Berger. PCCL. (Cited on page 29.)

[55] Dieter P. Gruber, Johannes Macher, and Gerald Berger. PCCL, 2010. (Cited on page 29.)

[56] Richard Stevens Burington and Donald Curtis Jr. May. *Handbook of probability and statistics with tables*. Handbook Publishers, Inc., Sandusky, Ohio, 1953. (Cited on page 30.)

[57] A. Azzalini and A. Dalla Valle. The multivariate skew normal distribution. *Biometrika Trust*, 83(4):715–726, December 1996. URL http://www.jstor.org/stable/2337278. last viewed on 2010-07-08. (Cited on pages 30 and 32.)

[58] Milton Ambramowitz and Irene A. Stegun, editors. *Handbook of mathematical functions*, volume 55. Dover Publications, Inc., December 1972. (Cited on page 32.)

[59] Tilo Arens, Frank Hettlich, Christian Karpfinger, Ulrich Kockelkorn, Klaus Lichtenegger, and Hellmuth Stachel. *Mathematik*. Spektrum Akademischer Verlag, Heidelberg, Germany, first edition, 2009. (Cited on page 33.)

[60] MATLAB® product help. *function differentiate*. The MathWorks Inc., R2009b. URL http://www.mathworks.com/access/helpdesk/help/toolbox/curvefit/differentiate.html. last viewed on 2010-07-08. (Cited on page 38.)

AFFIDAVIT

I declare in lieu of oath, that I wrote this thesis and performed the associated research myself, using only literature cited in this volume.

Leoben, May 2011

Dietmar Haba

— This thesis is dedicated to my little niece *Sophie-Christin Kohlendorfer*. —